Origin of basalts by hybridisation in andesite-dominated arcs

Michael Cassidy[1, 2*], Marie Edmonds[2], Sebastian F.L. Watt[1], Martin R. Palmer[1], Thomas M. Gernon[1]

1. Ocean and Earth Sciences, University of Southampton, National Oceanography Centre, European Way, Southampton, SO14 3ZH, UK

2. Department of Earth Sciences, University of Cambridge, Downing Street, Cambridge CB2 3EQ, UK.

* Corresponding author (m.cassidy@soton.ac.uk)

Running title: Hybridised basaltic volcanism

Keywords: Crystal zoning; Magma mixing; Melt inclusions; Tectonics; Mineral chemistry, Olivine, Magma chamber

ABSTRACT

Mafic magmas are common in subduction zone settings, yet their high density restricts their ascent to the surface. Once stalled in the crust, these magmas may differentiate, assimilate crust and other melts and mushes to produce hybridised intermediate magmas. The Soufriere Hills Volcano on Montserrat is a 'type locality' for these hybridisation processes and yet, just 3 km south of the crater, voluminous basalts have erupted from the South Soufriere Hills volcano within the same time period as the Soufriere Hills Volcano was erupting hybrid andesites (131 - 128 ka). Basaltic South Soufriere Hills magmas have 48 - 53 wt% SiO_2 and 4 - 6 wt% MgO. They were hot (970 - 1160 °C), volatile-rich (melt inclusions contain up to 6.2 wt% H_2O) and were stored at 8 – 13 km prior to eruption (based on olivine and pyroxene-hosted melt inclusion volatile geochemistry). Melt inclusions do not preserve basaltic liquids: they are andesitic to rhyolitic in composition, related to one another by a line of descent controlled by simple closed-system fractionation. Whole rock compositions, however, are best described by a hybridisation model involving "back"-mixing of andesitic to rhyolitic melts with mafic crystal phases such as magnetite, olivine, orthopyroxene and clinopyroxene. Phenocryst zoning illustrates repeated mixing events between evolved melts and mafic phenocrysts, which, when coupled with the heterogeneity of crystal compositions, strongly suggests that although the bulk composition is basalt (containing Fo_{80} olivine), they were assembled from disparate ingredients, likely derived from mafic crystal mushes and more evolved melt lenses of variable composition. The mixing events occur days to weeks prior to eruption. We propose that the South Soufriere Hills basaltic magmas, with their higher bulk density over andesites from neighbouring volcanoes, ultimately may have been eruptible owing to both the transtensional tectonics imposed by offshore grabens (related to the oblique subduction of the Lesser Antilles) and to surface unloading caused by large scale edifice collapse. Our observations support the idea that compositional changes in arcs might

reflect not only changes in source compositions, but also effects caused by patterns in crustal strain and tectonics.

INTRODUCTION

Intermediate magmas are generated by intensive crustal magmatic processing involving crystallisation, assimilation and mixing (Anderson, 1976; Eichelberger, 1978; Rudnick, 1995; Eichelberger et al. 2006; Reubi and Blundy, 2009; Kent et al., 2010; Melekhova et al., 2013). Mafic magmas are implicated in these processes through recharging of magma bodies by mingling at the interface and by large-scale overturn in magma reservoirs (Pallister et al., 1992; Bateman, 1995). These processes are well-illustrated by volcanoes in the Lesser Antilles arc where andesitic lavas containing mafic enclaves are commonly erupted. Andesites may erupt preferentially due to their relatively low density compared to the denser mafic lavas that are "trapped" at depth by a density filter mechanism (Plank and Langmuir, 1988). Rheological and lithological barriers may also inhibit the propagation of a basaltic melt (Eichelberger, 1978; Dufek and Begantz, 2005; Karlstrom et al., 2009; Kent et al., 2010). Indeed, intermediate to rhyolitic magma reservoirs can obstruct the passage of mafic magma, explaining why basaltic eruptions often only reach the surface on the periphery of silicic volcanoes (Hildreth, 1981). An interesting variant on this process is illustrated on Montserrat, where basalts were erupted from the South Soufrière Hills (SSH) volcano over the same broad time interval as crystal-rich andesites (with rhyolitic melts) were being erupted from the Soufrière Hills Volcano (SHV) located less than 3 km away. This raises the question as to what mechanisms allow eruption of felsic and mafic volcanic rocks in such close proximity.

More detailed study of the SSH is also of interest because, while there is strong evidence that andesites are generated largely by mixing of repeated injections of mafic magma into high level silicic magma chambers (Anderson, 1976; Eichelberger, 1978;

75 Eichelberger et al. 2006; Reubi and Blundy, 2009; Kent et al., 2010), the petrogenesis and
76 history of the mafic magmas is not well understood and may itself be complex. The density
77 filter trap (Plank and Langmuir, 1988) means that mafic enclaves from SHV are the only
78 evidence of deeper, mafic magmas that are available for petrologic analysis and in many
79 cases these mafic inclusions have experienced varying degrees of intrusion, quenching and
80 degassing that obscures their earlier characteristics. Thus, a study of closely spaced (in
81 distance and time) andesitic and basaltic volcanism at SHV and SSH has the potential to
82 reveal more detail regarding the nature of basaltic magmas resident in the mid- to upper-
83 crust, and can provide insights into the relative importance of magma mixing and
84 fractionation in controlling the composition of all arc volcanic rocks, and how this relates to
85 processes of magma storage, hybridisation, eruption triggering and growth of the arc crust.
86 In this paper we present new whole rock and melt inclusion analyses of basaltic to
87 andesitic lavas erupted from the SHV. We compare their geochemical characteristics to the
88 andesites erupted from SHV and examine the geochemistry of individual phenocrysts phases
89 to characterise compositional gradients related to normal crystal growth during cooling and
90 also due to mixing. We assess whether their compositions could have been generated by
91 simple processes of fractional crystallisation alone or whether mixing between disparate
92 liquid and mush components is necessary. Mineral melt thermometry has been used (from
93 two-pyroxenes and plagioclase-glass pairs) and barometry (using H_2O-CO_2 systematics of the
94 melt inclusions) to estimate pre-eruptive storage conditions. We use the relaxed
95 compositional steps across olivine crystals to infer pre-eruptive mixing timescales between
96 felsic liquids and mafic crystals. Using all of the available petrological and geochemical data
97 we develop a model for the generation of hybrid basalts on Montserrat and how they are
98 assembled and speculate as to the possible reasons for extraction and eruption of higher
99 density hybrid magmas relating to tectonics and unloading.

Geological background

The Lesser Antilles, like many arcs, comprises predominantly andesitic volcanic islands with relatively few basaltic centres. For example, in the northern and central islands (Saba to St. Lucia) <10% of the erupted volcanic rocks are basaltic. Where basaltic rocks are present, they generally occur as small-volume centres adjacent to much larger andesitic volcanoes (Westercamp and Mervoyer, 1976; Rea and Baker, 1980; Macdonald et al. 2000). This is exemplified on Montserrat (Fig. 1), where andesite lavas are predominant (Rea, 1974), with a single isolated basaltic centre (SSH) in the southernmost part of the island. Apart from the SSH, basalt occurrences are restricted to mafic inclusions within andesites. There is abundant petrological evidence (particularly from the currently active SHV) to show that the erupted andesites are hybrids formed over long timescales (10^3 to 10^4 years) by multiple recharges of deeply-sourced mafic magmas into large reservoirs of crystal-rich andesite magmas prior to ascent to the surface (Murphy et al., 2000; Humphreys et al., 2009; Plail et al., 2014).

The SSH basalts are, however, sufficiently geochemically distinct from the SHV basaltic enclaves suggesting that they reflect different magma sources and processes, such as increased relative contribution from slab fluids over subducted sediments (Zellmer et al., 2003; Cassidy et al., 2012; 2014), and thus provide information regarding magmas forming within the arc that are not generally observed, at least in an identifiable form, at the surface. Indeed, the SSH volcanic rocks represent some of the most mafic lavas in the northern Lesser Antilles arc (47 wt% SiO_2; 6 wt% MgO), with the exception of the high-Mg basalts in Martinique (Westercamp and Mervoyer, 1976). These geochemical differences are not simply related to temporal evolution of the volcanism on Montserrat, because Ar-Ar dating and stratigraphic relationships clearly indicate that the SSH and the SHV were both active in

125 the interval 130±5 ka (with SHV-type rocks forming the basal unit to the main SSH
126 lithologies), and the predominant andesitic volcanic rocks of the island were emplaced before
127 and after eruption of the SSH (Harford et al., 2002; Cassidy et al., 2012).

128 The island of Montserrat is located in the northern part of the Lesser Antilles; a 750
129 km long chain of volcanic islands formed as a result of the slow (2 cm yr^{-1}) subduction of the
130 North American plate beneath the Caribbean plate (Fig. 1) (Wadge, 1984; DeMets et al.,
131 2000). The oblique nature of this subduction means that the northern part of the arc is
132 influenced by transtensional forces that have led to intra-plate deformation (Feuillet, 2000;
133 Feuillet et al., 2010). Montserrat lies on crust ~30 km thick that sits on an asthenospheric
134 mantle wedge that extends to ~130 km in depth (Wadge and Shepherd, 1984). The island
135 comprises four volcanic centres: Silver Hills (2600-1200 ka), Centre Hills (950-550 ka), SHV
136 (282 ka to present) and SSH (131-128 ka) (Harford et al., 2002). All these volcanic centres
137 (except for the mafic-dominated SSH) are andesitic in composition, but their erupted
138 products all contain abundant inclusions of mafic magma (Rea, 1974; Murphy et al., 2000;
139 Zellmer et al., 2003; Barclay et al., 2010; Plail et al., 2014).

140 The SHV centre has been studied in most detail and is comprised of phenocrysts of
141 orthopyroxene, plagioclase and amphibole in a rhyolitic glass, with clear evidence for magma
142 mixing and mingling (Murphy et al., 2000; Humphreys et al., 2009; Humphreys et al., 2013).
143 Under-plating of the crystal-rich andesite by wet mafic magma causes instabilities to form at
144 the interface, forming enclaves (Plail et al., 2014; Edmonds et al., 2014), interspersed with
145 sporadic magma overturn events that thoroughly mix the magmas (Woods and Cowan, 2009),
146 distributing widely dispersed mafic components (Fe-rich plagioclase microlites, K-rich glass;
147 Humphreys et al., 2010) into the andesite body. The petrography and geochemistry of the
148 mafic enclaves of the SHV is also best explained by a mixing process between a mafic end
149 member (which varies in composition with time owing to lower crustal cryptic amphibole

fractionation) and variable amounts of rhyolitic melt hosting up to 20 vol% phenocrysts of plagioclase, amphibole and magnetite, although not in bulk rock proportions.

While there have been a large number of studies on the andesites of Montserrat, petrological work on the SSH basalts is more limited. Murphy et al. (2000) report that the mineral assemblage consists of plagioclase, olivine, clinopyroxene, and titanomagnetite. The SSH exposures comprise a range of rock suites from lava flows, to scoria, to reworked volcaniclastic material (Cassidy et al., 2014), with some more mafic enclaves and some lava flows containing cumulate xenoliths of orthopyroxene and plagioclase, similar to those described by Kiddle et al. (2010). The SSH exposures can be divided into two units on the basis of their distinct trace element and isotopic compositions: SSH Suite A has lower Sr/La and Sm/Zr ratios, but higher Zr/Er ratios and more radiogenic Pb isotope compositions than Suite B (Cassidy et al., 2014)

METHODS

Samples

Samples of SSH rocks were collected along the south coast of Montserrat (Fig. 1; Table 1). Splits were crushed using an agate Mortar and powdered for whole rock analysis and thin sections were also cut for electron microprobe (EMPA) and scanning electron microscope (SEM) analysis. Fractions of samples were crushed coarsely and crystals of enstatite, augite and olivine were picked from the 125-250 µm grain size fraction. The crystals were ground and polished to expose melt inclusions and mounted in indium for secondary ion mass spectrometry (SIMS) analysis. All the inclusions analysed were natural quenched, 40-200 µm in size and were not necked or breached by cracks.

Whole rock analysis

Major elements were analysed by X-ray Fluorescence (XRF) analysis of glass beads prepared by fusion of a mixture of 0.5 g subsamples and lithium tetraborate in a ratio of 1:10. Analyses were undertaken using a Philips Magix Pro WD-XRF at the National Oceanography Centre (NOC), Southampton, UK. Error and external accuracy was generally <2%.

Microanalysis (EMPA, SEM and SIMS)

Concentrations of H_2O and CO_2 in glass were obtained by SIMS on a Cameca IMF 4f ion microprobe at the NERC microanalytical facility at the University of Edinburgh, using a 15kV primary beam of O^- ions (Hauri et al., 2002; Blundy and Cashman, 2008). Positive secondary ions were accelerated to 4500 eV, with an offset of -75eV (for ^{1}H and trace elements) and -50eV (for ^{12}C) (± 20eV) to reduce transfer of molecular ions. A 50 µm raster was performed for three minutes prior to the start of each analysis, and a primary beam current of 5-6 nA used with a non-rastered, oval-shaped beam covering a 15-20 µm area on single spots within the boundaries of the melt inclusions. Peak positions were verified before each analysis. The following elements were analysed by counting for 3 s in each of a 10 cycle run: ^{1}H, ^{25}Mg, ^{30}Si. These counts were then normalised to ^{30}Si and converted to concentrations using a calibration curve populated by glass standards. The relative ion yield for H correlates with SiO_2 content, such that plotting $^{1}H/^{30}Si$ versus H_2O yields a single working curve for glasses of variable SiO_2 content. CO_2 concentrations, however, require a correction for SiO_2 content.

Carbon was measured independently of ^{1}H, using the same beam conditions, but with a 50 µm image field to improve transmission at moderate mass resolution, which was sufficient to resolve $^{24}Mg^{2+}$ at the ^{12}C peak position for background olivine measurements and inclusion analyses. ^{12}C was analysed for 3 s in each of 20 cycle runs in which $^{24}Mg^{2+}$, $^{28}Si^{2+}$ and ^{30}Si were also measured. During data processing, the first 5 cycles of the ^{1}H

200 analyses and the first 10 cycles of the ^{12}C data were discarded to avoid the effects of surface
201 contamination on the samples which may have survived the cleaning process. Instrumental
202 backgrounds were minimized by allowing samples held in epoxy to outgas in a separate
203 vacuum for at least ten hours prior to use in the SIMS instrument. The full list of glass
204 standards used is shown in suppl. Table 1. The accuracy and precision were monitored
205 throughout the sessions by repeat analysis of the standards as unknowns: for H_2O analyses
206 these were <9% and <6% respectively; and for CO_2 <11% and <8% respectively. The
207 average CO_2 and H_2O backgrounds over seven sessions were 56 ppm and 0.03 wt%
208 respectively. There is lack of variation between Al2O3 and MgO in melt inclusions
209 compositions, suggests that they do not follow the vectors anticipated for post-entrapment
210 crystallisation of the host mineral.

211 The major element and volatile (S, Cl and F) compositions of the glasses, inclusions
212 and phenocrysts were determined using the Cameca SX100 electron microprobe at the
213 University of Cambridge. Quantitative determinations of elements were made using the
214 wavelength dispersive system with TAP, PET and LIF crystals. A range of metal, oxide and
215 silicate (e.g. jadeite, wollastonite) standards was used for calibration of the spectrometers.
216 All analyses used an accelerating voltage of 15kV. For olivine, pyroxene and plagioclase a
217 spot size of 4 µm and a 100 nA beam current was used. For glasses, a 10 µm spot was used
218 with a beam current of 60 nA for Cl, F, S, P, Cr and Ni, and 4 nA for all other elements, with
219 counting times of 50-200 s per analysis. During glass measurements, Na peaks were counted
220 first to avoid significant migration during the run. In addition to calibration of each X-ray
221 line, a series of secondary reference standards (olivines, pyroxenes, feldspars and glasses)
222 were measured daily to check accuracy, precision and totals. Standards used were periclase
223 for Mg, jadeite for Na, fused Si for Si, rutile for Ti, fayalite for Fe, K-feldspar for K
224 corundum for Al, apatite for P, and pure metals for Cr and Mn. Repeat analyses of standards

were used to estimate the precision of An, Mg# and Fo measurements. Forsterite content of the St. John's Island Olivine standard was determined with a precision of 2σ=0·46 mol % (n=33). Precision of Mg# of clinopyroxene was similar to the precision of forsterite content in olivine. Anorthite content in the Anorthite55 standard was determined with a precision of 2σ=1·01 mol % (n=46).

Accuracy was generally better than 5% for most elements, based on repeat analyses of EMPA secondary standard 2390-5 and by comparison with reference concentrations for the standard, with the exception of TiO_2, K_2O, P_2O_5 and Cl, which were better than 20-35 %. Detection limits for S, Cl and F were 40, 38 and 170 ppm, respectively, and precision was typically < 5% for all oxides, with the exception of MnO, P_2O_5 and F, which was better than 20%.

Backscattered SEM images were taken at the NOC, using a LEO 1450VP (variable pressure) SEM. Carbon-coated samples were imaged at 15 kV, a working distance of 10 mm and a nominal probe current of 50–500 pA, using both secondary electron (SE) and backscattered electron (BSE) detectors.

RESULTS

The whole rock samples are black to grey in colour, and poorly to moderately vesicular (6-38%, average 20%). The SSH samples have bulk rock compositions ranging from basalt to andesite (47-58% SiO_2) (Table 1; Fig. 2). Also shown in Figure 2 are the compositions of andesites and mafic enclaves erupted from the SHV during 1995-2010, together with previously published data from SSH (Murphy et al,. 1998, 2000; Horwell et al., 2001; Zellmer et al., 2003; Humphreys et al., 2009, 2010; Cassidy et al., 2012). Relative to the SSH, the SHV volcanic rocks are more silicic, ranging from basaltic andesite to dacite

(53-68% SiO_2), but the SHV contain mafic enclaves that range from basaltic to basaltic andesite (49-55% SiO_2).

The SSH lavas are highly crystalline, with 31-53 vol.% phenocrysts and microphenocrysts (>100 □m) and 47-69% microlites. Plagioclase is the most abundant crystal phase (up to 61 vol.% of the crystal assemblage), followed by orthopyroxene (15 vol.%), olivine (11 vol.%) and clinopyroxene (10 vol.%), with titanomagnetite and rare amphibole in the basaltic andesite samples (SSH5B) comprising the remaining 3 vol.% (Fig. 3). The microlite crystal size fraction comprises a similar assemblage, however with less olivine present.

Olivine petrography

On average, olivines form the largest crystals (mean size 390 □m; range ±100 □m) and are often euhedral to subhedral. They are commonly fractured and slightly altered (slightly reddened along cracks, visible in plane polarised light). The forsterite contents (molar Fo% = Mg/(Mg+Fe) x 100) range from 56 to 80 mol. % (Figs. 4 and 5), with two main peaks in olivine core compositions (Fo_{72-80} in Group 1; Fo_{56-68} in Group 2) and two peaks in olivine rim compositions that are slightly less forsteritic than the cores. Most of the olivines are normally zoned or unzoned, but some exhibit reverse zoning (Fig. 6; Fig. 7), suggesting multiple magma bodies which have experienced mixing. The reverse-zoned olivines have core compositions of Fo_{71-80}, compared to Fo_{56-80} in the normally-zoned olivines (Figs. 5 and 6c). There is a negative correlation between olivine forsterite contents and CaO and MnO concentrations, with generally higher Fo% and lower Ca and Mn contents in the cores (Fig. 5). These correlations are significant at >95% confidence, with P-values <0.05. This correlation is especially strong between MnO and Fo% with a R^2 value of 0.9, but this correlation is less apparent with CaO and Fo% (R^2 of 0.36). The normally-zoned crystals show a trend of increasing Fo% from rim to core, mirrored by decreasing CaO and

MnO profiles (Figs. 6a and 6b). Figure 6d illustrates an olivine with reverse zoning towards the outer edge of the crystal, with a thin (<20 □m) band of normal zoning at the rim and no visible overgrowth. The core of this crystal has a constant forsterite composition of Fo_{72}, except for the outer 50 □m. The increase in forsterite content in the reverse zone is positively correlated with CaO, but negatively correlated with MnO content.

Plagioclase petrography

Plagioclase crystals range in size from microlites (<15 □m) to phenocrysts (>500 □m), with the latter commonly showing both normal and oscillatory zoning, as well as sieve textures (Fig. 3). Anorthite contents (An mol.% = Ca/(Ca+Na) x 100) range from 49-97% (Fig. 4). The feldspars are commonly normally-zoned, but with rare reverse-zoned phenocrysts also present (Fig. 7), suggesting a complex set of magmatic processes have occurred. The plagioclase crystals can be separated into two main groups based on their anorthite compositions. The cores and reverse-zoned rims are anorthitic (An_{79-97}), while the rims of the normally-zoned plagioclase are more albitic (An_{52-70}) and are generally richer in MgO, FeO and TiO_2 than the more anorthitic cores and rims (Fig.8). Complex dissolution and resorption is also seen in some crystals (Fig. 8b).

Pyroxene petrography

The average size of the orthopyroxene crystals is 142 □m ± 100 □m. They are commonly zoned and often occur as overgrowths on olivine (e.g. Fig. 6c). Magnesium number (Mg# = Mg/(Mg+Fe) x 100) ranges from 60-74 (Figs. 4 and 9), and all are enstatite in composition. Enstatite TiO_2 and Al_2O_3 contents generally decrease with decreasing Mg# (Fig. 9), but do not correlate significantly with Al/Ti ratios. The enstatite shows common reverse zoning and some normal zoning, but rare unzoned crystals are also present (Fig. 7).

Clinopyroxenes have an average crystal size of 176□□m ± 100 □m, with Mg# ranging from 58-80. The majority of the clinopyroxenes are augite, but some cores are

diopside . The augites are commonly zoned, but rare unzoned crystals also exist. Some of the clinopyroxene occurs as pigeonite overgrowths on the olivines (Figs. 6 and 10). Plots of Mg# versus minor elements (Fig. 9) show that the clinopyroxenes contain higher concentrations of TiO_2, Al_2O_3 and Al/Ti ratios than the enstatites. A traverse of a normally-zoned crystal shows complex saw tooth zoning (Fig. 10b) that is particularly oscillatory in the last 70 □m toward the rim, which occurs along with a sharp increase in Al_2O_3 and TiO_2 and a decrease in both Mg# and Al/Ti ratios.

Melt inclusion geochemistry

The melt inclusions are pristine, up to 90 □m in diameter, with no vapour bubbles and no daughter crystal phases. They span a range in compositions from andesitic to rhyolitic, with 58.2-72.6 wt.% SiO_2, 0.45-2.6 wt.% K_2O and 0.01-2.8 wt.% MgO (Fig. 2; Table 2). Their H_2O contents range from 1.50-6.19 wt.%, with CO_2 contents of 20-313 ppm (Fig. 11). CO_2 and S concentrations decrease with increasing melt SiO_2 contents, ranging from 395 ppm S and 313 ppm CO_2 at 58.2 wt.% SiO_2, to 18 ppm S and 20 ppm CO_2 at 72.6 wt.% SiO_2. Cl shows a positive relationship with SiO_2, ranging from 2500 ppm at 58.2 wt.% SiO_2 to 3610 ppm at 72.6 wt.% SiO_2.

DISCUSSION

The range of compositions and textures in mineral, whole-rock and melt inclusion chemistry suggests that the SSH mafic magma petrogenesis was just as complex as that observed for the SHV andesitic volcanic system on Montserrat and involved the assembly of multiple components. Here we discuss the origin of these components by considering the pressure-temperature conditions of magma storage, fractional crystallization and magma mixing that are reflected in the crystal and melt phases in the SSH erupted products, as well as the conditions required for the eruption of these products at the surface.

Pre-eruptive temperature, pressure and volatile content

Temperature estimates of the magma reservoir conditions are derived from the two-pyroxene thermometry and plagioclase-whole rock equilibria after applying the equilibrium test (where K_D = 1.09 ± 0.14 for pyroxene and 0.1 ± 0.11 for plagioclase) (Table 3; Putirka, 2008). The calculated temperature range of 970-1170 ºC is hotter than the estimates of the temperature for the neighbouring SHV magma reservoir, which is thought to reside at 840 ± 40 ºC based on experimental studies and pyroxene thermometry, heated by mafic magmas with temperatures of 900 ± 100 ºC (Devine et al., 1998; Barclay et al., 1998; Murphy et al. 2000; Devine et al. 2003; Humphreys et al., 2009) (Table 3). The SSH temperatures reported here were calculated on different samples and give a wide temperature range, which supports our argument that the erupted magma comprises components assembled from multiple magma bodies with differing storage conditions.

The melt inclusion data were used to estimate equilibration pressures using Volatilecalc (Newman and Lowenstern, 2002; Table 4). Most of the calculated pressures (using a temperature of 1000 ºC) range from 194-267 MPa, which equates to depths of 8.4-11.6 km (using an upper crustal density of 2300 kg/m^3; Hautmann et al., 2013), with one sample yielding a pressure of 25 MPa and a depth of 1.2 km. By comparison the magma stored beneath SHV is thought to reside in a dual reservoir system, one at 5-6 km depth, and the other at 10-12 km depth (Devine et al., 1998; Murphy et al., 1998; Barclay et al., 1998; Elsworth et al., 2008; Paulatto et al., 2010). With the exception of the low H_2O measurement (1.5 wt.%), which likely represents a melt inclusion that either equilibrated at shallow depth (1.2 km) or has lost H^+ by diffusive equilibration (Gaetani et al., 2012), the H_2O contents in the SSH melt inclusions lie at the upper range of H_2O contents (1.0-6.3 wt.%) measured in SHV melt inclusions (Humphreys et al., 2009; Mann et al., 2013; Edmonds et al., 2014). Thus, the high anorthite contents in the cores of the SSH plagioclase crystals (up to An_{97}) are

most likely due to the high dissolved H_2O contents (water contents exert a first order control on anorthite content and can elevate the anorthite contents to >An_{90}; Figure 4 in Lange et al., 2009).

Melt inclusion chemistry

With one exception, H_2O contents are approximately constant over the entire range of K_2O, SiO_2 and MgO concentrations (Fig. 11). At depths of 8-12 km, the exsolved vapour is likely to be CO_2-rich (Blundy et al., 2010), and the invariant water contents may thus reflect that the source of magmas hosting the phenocrysts erupted at SSH had similar primary H_2O contents (Tables 2 and 4). Cl concentrations are positively correlated with those of SiO_2, consistent with Cl behaving incompatibly with little or no degassing. Both CO_2 and S contents decrease with increasing SiO_2, indicating that these volatiles were progressively partitioned into a vapour phase as melts evolved. This is consistent with experimental data that suggests that oxidised arc rhyolites are associated with high vapour-melt partition coefficients for sulphur (Clemente et al., 2004; Zajacz et al., 2012). Similar melt inclusion trends have been observed in melt inclusion suites from Grenada which range from basalt to rhyolite and thought to be related by fractional crystallisation (Devine, 1995), as well as other examples from Kermadec arc (Haase et al., 2006; 2011; Barker et al., 2013), South Sandwich islands (Pearce et al., 1995), Mt Shasta (Grove et al., 2003) and from experimental studies (Sisson et al., 2005).

Figure 2 illustrates a comparison of melt inclusion and whole rock data from SSH and SHV with models of fractional crystallisation at pressures of 100-200 MPa under moderately oxidizing conditions using the AlphaMelts/RhyoliteMELTS model (Ghiorso and Sack 1995; Gualda et al., 2012). Two different scenarios are considered, the first models fractional crystallisation from a mafic bulk rock starting composition, and the second starts the model

373 from the most mafic melt inclusion composition. In the first, the starting composition is
374 defined by the most mafic of the SSH whole rocks (~47% SiO_2). The input parameters
375 include a fixed pressure (100 or 200 MPa), a starting temperature of 1200°C (as defined by
376 the two pyroxene thermometer above, and close to the calculated liquidus temperature from
377 RhyoliteMELTS) and an oxygen fugacity, f_{O2}, buffered at QFM+2 or NNO (Devine et al.,
378 1998; Murphy et al., 2000). The melt was then cooled at 50 °C intervals to simulate isobaric
379 fractional crystallization involving olivine, plagioclase, magnetite, augite, enstatite and
380 amphibole (Table 2, Fig. 2).

381 Regardless of the pressure or f_{O2}, simple isobaric fractional crystallization predicts
382 non-linear liquid lines of descent that fail to reproduce the simple linear trends defined by the
383 majority of the whole rock data. Hence, the range in whole rock data from both SSH and
384 SHV are best described by a hybridization model in which the rocks are mixtures between
385 andesitic to rhyolitic melts and mafic crystal phases, as observed in many other arc volcanic
386 settings (Davidson et al., 2005; Reubi and Blundy, 2009; Kent et al, 2010; Cashman and
387 Blundy, 2013; Humphreys et al., 2013; Cooper and Kent, 2014).

388 In contrast, a fractional crystallisation history can explain most of the melt inclusions
389 from SSH, and a significant proportion of those from SHV. These melt inclusions do not lie
390 on the linear trend defined by the whole rock data. For the melt inclusions, the best fit to the
391 AlphaMelts/RhyoliteMELTS model (Ghiorso and Sack 1995; Gualda et al., 2012) is provided
392 by a scenario in which the starting composition is defined by the most mafic of the SSH melt
393 inclusions (58.7% SiO_2). The input and cooling parameters are the same as for the first
394 modelling scenario above and, again, the effects of pressure and f_{O2} do not yield major
395 variation in the liquid line of descent (Fig. 2).

396 To summarise, the melts are related to one another by fractionation crystallisation and
397 likely evolve in closed systems in storage lenses in the crust. The bulk basaltic lavas are

398 “assembled” by mixing liquids along this line of descent with mafic crystal mushes
399 containing mixtures of plagioclase, olivine and clinopyroxene. The whole rocks therefore
400 represent hybrids or mixtures between melts and mush components. In detail, it can be
401 observed that most of the melt inclusion liquids are in equilibrium with their host crystals
402 (Table 2), which means that at the time of melt entrapment, the crystal and its carrier liquid
403 were in equilibrium. The crystals are strongly zoned however, and the melts are therefore not
404 necessarily in equilibrium with other parts of the crystal, or with other crystals in the magma.
405 The melt inclusions were trapped over a pressure range corresponding to depths of
406 between 8 and 12 km (Table 4). We speculate that the more mafic liquids are sourced from
407 the deeper parts of the magma reservoir system. In contrast to SHV, the crystal assemblage at
408 SSH is markedly more mafic, likely derived from deeper in the crust. For the basalts of the
409 SSH, the depths recorded from volatile solubilities in melt inclusions suggest that melt
410 entrapment occurs at the deeper end of the range estimated for the SHV system Edmonds et
411 al., (2014), thus preserving a greater range of melt inclusion compositions (from andesite to
412 rhyolite), further suggesting that in general melts become more evolved upward through the
413 crust. This is supported by a broad negative correlation in the melt inclusion data, between
414 SiO_2 and equilibration pressure (R^2= 0.45), indicating that the least evolved compositions
415 were generally formed at deeper depths.
416 It is important to note that the record of pressures recorded by the melt inclusions is
417 itself subject to bias. The depths of melt entrapment are probably governed not only by the
418 physical dimensions of the reservoir but also and perhaps more importantly by the conditions
419 under which melt inclusions form, which requires both high degrees of undercooling and a
420 period of isothermal crystal growth (Kohut and Nielsen, 2004; Kent et al., 2008). Mafic
421 phenocrysts may have not experienced sufficient undercooling, until mixing, by which time

422 the compositions had been modified by time isothermal crystallisation occurs and melt
423 inclusions become trapped (Koleszar et al., 2012).

424 Mixing is well documented in other arc systems. A notable example of the mixing
425 process described above is associated with the Mount St Helens dacite, where temperature
426 fluctuations of 20-40 °C were a consequence of incremental, or pulsed assembly of crustal
427 magma bodies wherein each pulse interacts with ancestral, stored magmas, accounting for
428 much of the plagioclase zoning and textural complexity seen in the erupted magmas
429 (Cashman and Blundy, 2013). These authors suggest that magma storage systems under most
430 arc volcanoes are dominated by similar processes, where crystal mushes are fed by hotter,
431 slightly more mafic magma, coupled with episodes of magma ascent from one storage region
432 to another. The presence of common enclaves of cumulate material, such as gabbro and
433 pyroxenite, in the SSH lavas (Cassidy et al., 2014) is also consistent with the remobilisation
434 of plutonic material. The way in which the model we propose differs from this fundamental
435 mixing scenario is that we propose "back-mixing" to generate mafic bulk compositions by
436 mixing more evolved melts with mafic mushes, illustrating the importance of not only
437 mushes, but also regions of andesitic to rhyolitic liquids in magma reservoirs for generating
438 bulk compositions.

439 *Textural evidence for mixing*

440 The olivine, plagioclase and pyroxene phenocryst compositional profiles all record
441 normal and reverse zoning, suggesting a combination of growth zoning and magma mixing
442 (Figs. 6, 7, 8 and 11). Major element mineral chemistry is modified during growth in
443 response to cooling, melt compositional changes and magma reservoir conditions; including
444 pressure, temperature, volatile content and f_{O2} (Housh & Luhr 1991; Nelson & Montana,
445 1992; Sisson and Grove, 1993; Couch et al., 2003a, 2003b; Streck, 2008; Cashman and
446 Blundy 2013). Minor element concentrations are particularly useful for discriminating

between magma mixing and growth zoning, as they are almost entirely a function of melt composition and are largely unaffected by changes in magma storage conditions (Ruprecht and Worner, 2007; Aigner-Torres et al., 2007).

Zoning profiles in plagioclase crystals shows that anorthite contents are negatively correlated with Fe, Mg and Ti (Fig. 8), with magma crystallisation and differentiation yielding less An-rich compositions, and increases in magma temperature or water content raising An contents. Although Fe partitioning in plagioclase strongly depends on crystal composition, and melt temperature and f_{O2} (Longhi et al., 1976; Sugawara, 2001; Aigner-Torres et al., 2007), melt composition has the greatest effect on Fe plagioclase content (Ginibre et al., 2002). By comparison, experimental data show a clear negative correlation between Ti and An% that is largely independent of temperature, and Mg partitioning depends weakly on An content (Bindeman et al., 1998) and temperature (Longhi et al., 1976; Aigner-Torres et al 2007). Therefore, changes in An content, temperature, f_{O2} alone cannot fully replicate the observed increases in Fe, Mg and Ti observed at the rim of the crystals (Fig. 8). Rather, these observations suggest that the increases in these elements must be due, at least in part, to disequilibrium crystallisation prior to eruption as a result of mixing with melts enriched in Fe, Mg and Ti. This interpretation is supported by the kernel density plots of anorthite content (Fig. 4), where two populations of cores are evident, as well as a large range of anorthite values at the rims. The population of cores with An_{76-95} likely represents deeper, more stable plagioclase crystallisation, but the cores with lower anorthite contents (An_{50-65}) may represent plagioclase crystals that evolved in a shallower (lower PH_2O), more evolved, magma body. Zoning profiles (Figure 8a) show cores with high anorthite contents (An_{86}) and increasingly albitic rims (down to An_{56}) with a corresponding increase in Fe, Mg and Ti contents.. This zoning profile is consistent with a plagioclase from a wet mafic mush being mixed into a more evolved melt at lower pressures.

A history of mixing is supported by the presence of two distinct groups in olivine core compositions (Figs. 4 and 5): Group 1, Fo_{72-80} and Group 2, Fo_{56-68}. These groups suggest mixing between two distinct magma batches, or with the entrainment of more forsteritic olivines from a crystal mush into a more evolved crystal-rich magma. The olivine crystals (both Group 1 and Group 2) exhibit both normal (most common) and reverse zoning at the rim of the crystal (Figs. 5c, 6, 7 and 12a). Many of the Group 1 olivines exhibit normal zoning at the rims, consistent with magma from a primitive mush entrained into a more evolved storage system. This hypothesis is illustrated by the zoning profile in Figure 6b, which contains shows a Group 1 olivine with a lower forsterite, but higher Ca and Mn rim. Simple fractional crystallisation would reduce the CaO content along with Fo content, but while Ca and Mn partitioning are not directly affected by melt f_{O2} and temperature (Dunn, 1987; Libourel, 1999), Ca concentration of olivines is strongly dependent on the alkali composition of the melt (Jurewicz and Watson, 1988; Libourel, 1999). Mixing of the Group 1 olivines into an evolved melt with a higher alkali content may therefore explain the observed increased Ca content with decreasing Fo. The reverse zoning observed in some of the Group 2 olivines is consistent with olivine from the partially crystalline andesite being exposed to more mafic compositions and hotter temperatures of the intruding magma.

Pyroxene Mg# can change in response to changes in melt composition or f_{O2} (Streck et al., 2002). Thus, the saw-tooth major element zoning in Figure 10 is likely related to a combination of open system fractionation and recharge (Ginibre et al., 2002; Ruprecht and Worner, 2007), while the relatively large increases in Mg# approaching the rims (the outer 40 µm) of a fraction (~5%) of the pyroxenes are consistent with a change in the composition and/or temperature of the intruding mafic magma (Fig. 10). Indeed, similar orthopyroxenes have been erupted at SHV eruption since May 1996, with well-developed reverse zoned rims (10–25 µm) (Murphy et al., 2000).

Timing of mixing events

The mixing of a phenocryst into a melt of a different composition would lead to a sharp step in the mineral composition crystallising at the rim, assuming that conditions for crystal growth are maintained and that the mixing event results in an instantaneous, rather than gradual, change in the composition of the host melt. This sharp step then relaxes over time, via diffusion, as the interior of the crystal begins to equilibrate with its new host melt composition. The resulting diffusion profiles may be used to estimate the timescales between magma mixing and eruption, by assuming a particular temperature (Costa and Chakraborty, 2004 Morgan et al., 2004; Costa and Dugan, 2005; Costa et al., 2008). This diffusion chronometric approach has been applied to reverse zoning profiles in our SSH samples (we cannot apply it to normal zoning profiles, because it is difficult to distinguish mixing-driven disequilibrium from fractionation-dependent growth zoning in this case). We use the DIPRA model (Girona and Costa, 2013) for both forsterite and Mn zoning, at 1000°C. The shapes of the compositional profiles in the reverse zones at the rims of two olivines (Fig. 5b) are consistent with relaxation of an initial compositional step over 10 to 60 days (Supplementary figures 1 and 2). This timescale is similar to that estimated from compositional profiles in Fe-Ti oxides induced by heating in SHV lavas, where andesite remobilisation by mafic intrusions occurred days to weeks prior to eruptions (Devine et al., 2003). A timescale of days to weeks between mixing and eruption is comparable to the short pre-eruptive mixing timescales calculated at Ceboruco, Quizapu, Nea Kamini and Mount Unzen volcanoes (days to months; Nakamura, 1995; Chertkoff and Gardner, 2004; Ruprecht and Cooper, 2012; Martin et al., 2008). Other mixed systems at Trident, Taupo and Volcan San Pedro, give longer timescales (months to decades; Coombs et al. 2000; Costa and Chakraborty, 2004; Millet et al., 2014). Our results imply a relatively short period between the assembly of the SSH magmas and their ascent and eruption at the surface.

Formation of basaltic magmas at the SSH

Basalts are often thought to represent relatively unmodified primary melts from the mantle. However observations in this study from whole rock trends, melt inclusions, fractional crystallisation modelling and phenocryst zoning attest to a hybridisation model similar to that previously inferred for the formation of andesites at many intermediate systems. Magma mixing commonly occurs between mafic and felsic melts to form andesitic compositions, following the recharge filtering model of Kent et al. (2010). However, the basaltic whole rock compositions of SSH are generated mixing components from multiple magma bodies, comprising andesitic to rhyolitic melt compositions and mafic mineral phases. The SSH preserves a wide range of melt inclusion compositions unlike the SHV which comprises only limited range of evolved rhyolitic melt inclusions. This is likely a consequence of the deeper mixing of multiple different magma bodies and the lack of a further shallow crystallisation stage, which would otherwise increase the likelihood of preserving silicic melt inclusions through the incorporation of crystals derived from a shallow crystal mush.

Tectonic control for the eruption of basalts

While many of the observations relating to magma mixing as a control over whole rock and melt inclusion compositions have been well-documented in arc volcanic rocks (Reubi and Blundy, 2009), they do not explain the closely-spaced and near coeval eruption of basaltic and andesite lavas at SSH and SHV ~130 ka. In this context, it is noteworthy that the volatile contents of melt inclusions and geophysical investigations of SHV support the existence of two upper crustal magma chambers; one at 10-12 km that feed into a shallower chamber at 5-6 km depth that serves as the source of the erupted material (Devine et al., 1998; Barclay et al., 1998; Elsworth et al., 2008; Humphreys et al., 2009; Paulatto et al., 2010; Mann et al., 2013; Edmonds et al., 2014). We hypothesise that the eruption of more

547 mafic rocks at SSH was because these lavas were assembled directly from a magma chamber
548 of similar depth (8-12 km) to the deeper of the two chambers below SHV, but without
549 passing through the shallower chamber. But what allows the SSH basalts to bypass this
550 shallow density filter?

551 In general, eruption of basaltic compositions in dominantly andesitic settings requires
552 a favourable stress field (Hildreth, 1981). Indeed, density is not the only factor which limits
553 the ascent of mafic magmas; structural controls imposed by lithology and rheological
554 boundaries within the crust can also act to slow and sometimes stall magma ascent
555 (Eichelberger, 1978; Dufek and Bergantz, 2005; Karlstrom et al 2009; Kent et al., 2010).
556 Faulting systems may promote the ascent of denser magmas, particularly within an
557 extensional and therefore decompressional regime. Volcanoes are also commonly found
558 along major strike-slip faults, such as the great Sumatran fault zone, the Sulawesi fault and
559 the Liquiñe–Ofqui fault zone (LOFZ) in Chile (Bellier and Sébrier, 1994; Lécuyer et al.,
560 1997; Cembrano and Lara, 2009). In these areas, local extensional features are associated
561 with individual volcanoes, and it is suggested that a causal relationship exists between
562 extension and volcanism or intrusion (Moore, 1979; Aydin and Nur, 1982; Hutton and
563 Reavey, 1992; Tibaldi, 1992; Milia and Torrente, 2003; Spinks et al. 2005; Brogi et al. 2010;
564 Davis et al. 2010). In addition, there is evidence that tectonics can strongly control the
565 composition of magmas. For instance, at the Taupo volcanic zone basaltic volcanism occurs
566 at the intersection between major faults and caldera boundaries (Cole et al., 1990; Millet et al.
567 2014) whereas, more intermediate magmatism occurs in areas which have experienced less
568 crustal extension (Allan et al. 2013 ; Millet et al. 2014), following the recharge filtering
569 process. Transtensional faults in the neighbouring island to Montserrat, Guadeloupe, which
570 lies along the same en echelon fault system, are thought to control the location of volcanism
571 and may be the cause for the frequent sector collapses on the island (Mathieu et al., 2011).

572 Transtensional tectonics in this region may not only control the source of these magmas
573 (Cassidy et al., 2012), but may also lead to localised faulting that thus provides a pathway for
574 these higher density mafic magmas, that would otherwise be trapped within the crust (Fig.
575 12). Over time, however, the crust in these areas may impose lithostatic control as the
576 eruption of the basalts thickens the crust. As a result, later magmas would be required to
577 undergo differentiation by crystal segregation to become buoyant enough to erupt at the
578 surface (Plank and Langmuir, 1988; Devine, 1995), thus increasing the likelihood of
579 generating more evolved andesites. This is supported by numerical modelling from Pinel and
580 Jaupart (2000), which predicts that as the edifice grows the ascension of lower density
581 magma is favoured, thus promoting stalling in the crust and magma differentiation. Hence,
582 the eruption of basaltic lavas may be characteristic of the early products of new eruption
583 centres where extensional tectonics are operative in arc settings. This may be the case for
584 many volcanic regions which comprise early phases of basaltic activity before evolving into
585 mature andesitic systems, including northern Japan (Katsui et al., 1978; 1979); central south
586 Chile (Lopez-Escobar et al., 1977), New Zealand (Price et al., 2005), the Aleutians and
587 Alaska (Marsh, 1980; Myers and Marsh, 1981). The role of transtensional tectonics is
588 strengthened by the observation that both Redonda and Kahouanne, two adjacent islands to
589 Montserrat which lie on the same transtensional fault systems (Fig. 1), also produce mafic
590 volcanism. These seamounts represent the emergence of new volcanism in the Lesser
591 Antilles, and again suggest that early arc volcanism in this region may be controlled by
592 tectonics, until further growth of the edifice inhibits the ascent of high density mafic magmas,
593 producing the commonly observed andesitic volcanoes. Although fault structures thus
594 provide a possible mechanism for promoting the ascent of the SSH magmas, this alone does
595 not explain the timing of SSH basaltic magmatism. Basaltic eruptions have not been
596 identified at other periods in Montserrat's history. The conditions favourable to basaltic

eruptions at SSH thus appear to have been transient, and are unique in the currently identified history of Montserrat. The SSH doesn't clearly correspond to an initial phase of volcanism, in the sense of the birth of a new volcanic centre, since the event is bracketed by andesite eruptions at the adjacent SHV, and there have been no subsequent eruptions (since 130 ka) at SSH. We know of no reasons why fault activity at the time of SSH volcanism would have been enhanced relative to other periods in Montserrat's history. Thus, although fault structures may have promoted ascent of dense mafic magmas at this location, this alone does not provide a satisfactory explanation for the timing of the SSH episode of basaltic volcanism. Other processes affecting crustal stress conditions, such as collapse of the volcanic edifice, may help explain the precise timing of SSH volcanism.

CONCLUSIONS

There is now abundant evidence that arc andesites are generated by hybridisation processes, involving the mixing of felsic melts and abundant crystal phases, for instance at the SHV on Montserrat, Mt St Helens and at Mount Hood (USA). Arc basalts, on the other hand, are commonly attributed to simple closed-system fractionation. Our study of the SSH, shows that olivine-bearing basalt petrogenesis can be just as complex as the generation of andesites at the SHV, implying that basalts in arcs may have a less simple history than is commonly assumed on account of the hybridisation processes explored in this study.

This study also shows how two volcanoes active at similar times and located very close to each other can erupt different bulk compositions. Basalts erupted from the SSH in Montserrat were stored under different magmatic conditions to the andesites of the SHV, yet underwent similar magmatic processes of mixing, recharge and cumulate entrainment prior to eruption. The range of magmatic temperature estimates (970 - 1160˚C), reservoir depth

estimates (8-12 km), coupled with crystal and whole rock compositions, strongly indicates the presence of multiple magma bodies, which interact and feed basaltic eruptions. Melt inclusion data, phenocryst chemistry and fractional crystallisation modelling suggests that mixing and crystal entrainment were involved in the petrogenesis of the SSH mafic magmas. The SSH magmatic system seems to match the deeper mafic-proposed SHV magma reservoir, but geophysical and petrological studies suggest that this deeper SHV system is much larger in volume than the shallow SHV reservoir. This is in contrast with the SSH, the results here show evidence for small, discrete pockets of crystal mushes with melt batches, which might appear in geophysical surveys as one large reservoir. We suggest that ascent of mafic magmas can be promoted by tectonics, which may ascend along faults or under specific stress conditions (i.e. post collapse).

Acknowledgements

Iris Buisman, Ian Croudace, Richard Pearce are thanked for lab assistance. The authors wish to thank Adam Kent, Marc-Alban Millet and Jim Cole for their constructive reviews and for the editorial handling of John Gamble. MC and SFLW thank NERC for financial support via grant NE/K000403/1.

REFERENCES

Aigner-Torres, M., J. Blundy, P. Ulmer, and T. Pettke. "Laser Ablation Icpms Study of Trace Element Partitioning between Plagioclase and Basaltic Melts: An Experimental Approach." *Contributions to Mineralogy and Petrology* 153, no. 6 (2007): 647-667.

Allan, A. S. R., Morgan, D. J., Wilson, C. J. N. & Millet, M. A. (2013). From mush to eruption in centuries: assembly of the super-sized Oruanui magma body. *Contributions to Mineralogy and Petrology* **166**, 143-164.

Anderson, P. "Oceanic-Crust and Arc-Trench Gap Tectonics in Southwestern British-Columbia." *Geology* 4, no. 7 (1976): 443-446.

Annen, C., Blundy, J.D., and Sparks, R.S.J., 2006, The genesis of intermediate and silicic magmas in deep crustal hot zones: Journal of Petrology, v. 47 pp. 505-539 doi: 10.1093/petrology/egi084.

Aydin, A., and A. Nur. "Evolution of Pull Apart Basins and Their Scale Independence." *Tectonics* 1, no. 1 (1982): 91-105.

Barclay, J., M. J. Rutherford, M. R. Carroll, M. D. Murphy, J. D. Devine, J. Gardner, and R. S. J. Sparks. "Experimental Phase Equilibria Constraints on Pre-Eruptive Storage Conditions of the Soufriere Hills Magma." *Geophysical Research Letters* 25, no. 18 (1998): 3437-3440.

Barclay, J., Herd, R.A., Edwards, B., Kiddle, E., Donovan, A. (2010). Caught in the act: implications for the increasing abundance of mafic enclaves during the eruption of the Soufriere Hills Volcano, Montserrat.Geophyscial Research Letters, Vol. 37, L00E09, 5 PP., 2010 doi:10.1029/2010GL042509.

671 Barker, S. J., C. J. N. Wilson, J. A. Baker, M. A. Millet, M. D. Rotella, I. C. Wright, and R. J.
672 Wysoczanski. "Geochemistry and Petrogenesis of Silicic Magmas in the Intra-
673 Oceanic Kermadec Arc." *Journal of Petrology* 54, no. 2 (2013): 351-391.
674
675 Bateman, R. "The Interplay between Crystallization, Replenishment and Hybridization in
676 Large Felsic Magma Chambers." *Earth-Science Reviews* 39, no. 1-2 (1995): 91-106.
677
678 Bellier, O., and M. Sebrier. "Relationship between Tectonism and Volcanism Along the
679 Great Sumatran Fault Zone Deduced by Spot Image Analyses." *Tectonophysics* 233,
680 no. 3-4 (1994): 215-231.
681
682 Bindeman, I. N., A. M. Davis, and M. J. Drake. "Ion Microprobe Study of Plagioclase-Basalt
683 Partition Experiments at Natural Concentration Levels of Trace Elements."
684 *Geochimica Et Cosmochimica Acta* 62, no. 7 (1998): 1175-1193.
685
686 Blundy, J., and K. Cashman. "Petrologic Reconstruction of Magmatic System Variables and
687 Processes." In *Minerals, Inclusions and Volcanic Processes*, edited by K. D. Putirka
688 and F. J. Tepley, 69, 179-239, (2008).
689
690 Blundy, J., Cashman, K.V., Rust, A., Witham, F., 2010. A case for CO2-rich arc magmas.
691 Earth Planet. Sci. Lett. 290, 289-301.
692
693 Brogi, A., E. Capezzuoli, R. Ague, M. Branca, and M. Voltaggio. "Studying Travertines for
694 Neotectonics Investigations: Middle-Late Pleistocene Syn-Tectonic Travertine

695 Deposition at Serre Di Rapolano (Northern Apennines, Italy)." *International Journal*
696 *of Earth Sciences* 99, no. 6 (2010): 1383-1398.
697
698 Cashman, K., and J. Blundy. "Petrological Cannibalism: The Chemical and Textural
699 Consequences of Incremental Magma Body Growth." *Contributions to Mineralogy*
700 *and Petrology* 166, no. 3 (2013): 703-729.
701
702 Cassidy, M., Taylor, R. N., Palmer, M. R., Cooper, R. J., Stenlake, C., Trofimovs, J.
703 "Tracking the Magmatic Evolution of Island Arc Volcanism: Insights from a High-
704 Precision Pb Isotope Record of Montserrat, Lesser Antilles." *Geochemistry*
705 *Geophysics Geosystems* 13, (2012).
706
707 Cassidy, M., Trofimovs, J., Watt, S.F.L., Palmer, M.R., Taylor, R.N., Gernon, T.M., Talling,
708 P.J., Le Friant, A. "Multi-Stage Collapse Events in the South Soufrière Hills,
709 Montserrat, as Recorded in Marine Sediment Cores." In *The Eruption of Soufrière*
710 *Hills Volcano, Montserrat from 2000 to 2010*, edited by G. Wadge, Robertson, R.,
711 Voight, B.,: Memoir of the Geological Society, London 2014.
712
713 Cembrano, J., Lara, L., 2009. The link between volcanism and tectonics in the southern
714 volcanic zone of the Chilean Andes: A review. Tectonophysics 471, 96-113.
715
716 Chertkoff, D. G. & Gardner, J. E. (2004). Nature and timing of magma interactions before,
717 during, and after the caldera-forming eruption of Volcaan Ceboruco, Mexico.
718 *Contributions to Mineralogy and Petrology* **146**, 715-735.
719

720 Clemente, B., Scaillet, B., Pichavant, M., 2004. The solubility of sulphur in hydrous rhyolitic
721 melts. Journal of Petrology 45, 2171-2196.
722
723 Cole, J. W. (1990). Structural control and origin of volcanism in the Taupo Volcanic Zone,
724 New Zealand. *Bulletin of Volcanology* **52**, 445-459.
725
726 Coombs, M. L., Eichelberger, J. C. & Rutherford, M. J. (2000). Magma storage and mixing
727 conditions for the 1953-1974 eruptions of Southwest Trident Volcano, Katmai
728 National Park, Alaska. *Contributions to Mineralogy and Petrology* **140**, 99-118.
729
730 Cooper, K. M., Kent, A.J.R. "Rapid Remobilization of Magmatic Crystals Kept in Cold
731 Storage." *Nature* 506, (2014): 480-483.
732
733 Costa, F., and S. Chakraborty. "Decadal Time Gaps between Mafic Intrusion and Silicic
734 Eruption Obtained from Chemical Zoning Patterns in Olivine." *Earth and Planetary*
735 *Science Letters* 227, no. 3-4 (2004): 517-530.
736
737 Costa, F., R. Dohmen, and S. Chakraborty. "Time Scales of Magmatic Processes from
738 Modeling the Zoning Patterns of Crystals." In *Minerals, Inclusions and Volcanic*
739 *Processes*, edited by K. D. Putirka and F. J. Tepley, 69, 545-594, 2008.
740
741 Costa, F., and M. Dungan. "Short Time Scales of Magmatic Assimilation from Diffusion
742 Modeling of Multiple Elements in Olivine." *Geology* 33, no. 10 (2005): 837-840.
743

744 Couch, S., C. L. Harford, R. S. J. Sparks, and M. R. Carroll. "Experimental Constraints on the
745 Conditions of Formation of Highly Calcic Plagioclase Microlites at the Soufrire Hills
746 Volcano, Montserrat." *Journal of Petrology* 44, no. 8 (2003a): 1455-1475.
747
748 Couch, S., R. S. J. Sparks, and M. R. Carroll. "The Kinetics of Degassing-Induced
749 Crystallization at Soufriere Hills Volcano, Montserrat." *Journal of Petrology* 44, no. 8
750 (2003b): 1477-1502.
751
752 Davidson, J. P., J. M. Hora, J. M. Garrison, and M. A. Dungan. "Crustal Forensics in Arc
753 Magmas." *Journal of Volcanology and Geothermal Research* 140, no. 1-3 (2005):
754 157-170.
755
756 Davis, A. S., D. A. Clague, J. B. Paduan, B. L. Cousens, and J. Huard. "Origin of Volcanic
757 Seamounts at the Continental Margin of California Related to Changes in Plate
758 Margins." *Geochemistry Geophysics Geosystems* 11, (2010).
759
760 DeMets, C., P. E. Jansma, G. S. Mattioli, T. H. Dixon, F. Farina, R. Bilham, E. Calais, and P.
761 Mann. "Gps Geodetic Constraints on Caribbean-North America Plate Motion."
762 *Geophysical Research Letters* 27, no. 3 (2000): 437-440.
763
764 Devine, J. D. "Petrogenesis of the Basalt-Andesite-Dacite Association of Grenada, Lesser
765 Antilles Island Arc, Revisited." *Journal of Volcanology and Geothermal Research* 69,
766 no. 1-2 (1995): 1-33.
767

Devine, J. D., M. D. Murphy, M. J. Rutherford, J. Barclay, R. S. J. Sparks, M. R. Carroll, S. R. Young, and J. E. Gardner. "Petrologic Evidence for Pre-Eruptive Pressure-Temperature Conditions, and Recent Reheating, of Andesitic Magma Erupting at the Soufriere Hills Volcano, Montserrat, Wi." *Geophysical Research Letters* 25, no. 19 (1998): 3669-3672.

Devine, J. D., M. J. Rutherford, G. E. Norton, and S. R. Young. "Magma Storage Region Processes Inferred from Geochemistry of Fe-Ti Oxides in Andesitic Magma, Soufriere Hills Volcano, Montserrat, Wi." *Journal of Petrology* 44, no. 8 (2003): 1375-1400.

Dixon J.E. 'Degassing of alkalic basalts' *American Mineralogist*, 82 (1997), pp. 368–378

Dufek, J. & Bergantz, G. W. (2005). Lower crustal magma genesis and preservation: A stochastic framework for the evaluation of basalt-crust interaction. *Journal of Petrology* **46**, 2167-2195.

Dunn, T. "Partitioning of Hf, Lu, Ti, and Mn between Olivine, Clinopyroxene and Basaltic Liquid." *Contributions to Mineralogy and Petrology* 96, no. 4 (1987): 476-484.

Edmonds, M, Humphreys, MCS, Hauri, E, Herd, R, Wadge, G, Rawson, H, Ledden, R, Plail, M, Barclay, J, Aiuppa, A, Christopher, T, Giudice, G & Guida, R, ed. *Pre-Eruptive Vapour and Its Role in Controlling Eruption Style and Longevity at Soufriere Hills Volcano*. Edited by G Wadge, Robertson, R & Voight, B, The Eruption of Soufriere Hills Montserrat from 2000 to 2010: The Geological Society of London, 2014.

Eichelberger, J. C. "Andesitic Volcanism and Crustal Evolution." *Nature* 275, no. 5675 (1978): 21-27.

Eichelberger, J. C., P. E. Izbekov, and B. L. Browne. "Bulk Chemical Trends at Arc Volcanoes Are Not Liquid Lines of Descent." *Lithos* 87, no. 1-2 (2006): 135-154.

Elsworth, D., G. Mattioli, J. Taron, B. Voight, and R. Herd. "Implications of Magma Transfer between Multiple Reservoirs on Eruption Cycling." *Science* 322, no. 5899 (2008): 246-248.

Feuillet, N. "Sismotectonique Des Petites Antilles, Liason Entre Activite Sismique Et Volcanique = Sismotectonics of Lesser Antilles, Relationship between Seismic Activity and Volcanism." Rene Diderot University, 2000.

Feuillet, N., F. Leclerc, P. Tapponnier, F. Beauducel, G. Boudon, A. Le Friant, C. Deplus, J. F. Lebrun, A. Nercessian, J. M. Saurel, and V. Clement. "Active Faulting Induced by Slip Partitioning in Montserrat and Link with Volcanic Activity: New Insights from the 2009 Gwadaseis Marine Cruise Data." *Geophysical Research Letters* 37, (2010): 6.

Gaetani, G. A., J. A. O'Leary, N. Shimizu, C. E. Bucholz, and M. Newville. "Rapid Reequilibration of H2o and Oxygen Fugacity in Olivine-Hosted Melt Inclusions." *Geology* 40, no. 10 (2012): 915-918.

816 Ghiorso, M. S., and R. O. Sack. "Chemical Mass-Transfer in Magmatic Processes .4. A
817 Revised and Internally Consistent Thermodynamic Model for the Interpolation and
818 Extrapolation of Liquid-Solid Equilibria in Magmatic Systems at Elevated-
819 Temperatures and Pressures." *Contributions to Mineralogy and Petrology* 119, no. 2-
820 3 (1995): 197-212.
821
822 Ginibre, C., G. Worner, and A. Kronz. "Minor- and Trace-Element Zoning in Plagioclase:
823 Implications for Magma Chamber Processes at Parinacota Volcano, Northern Chile."
824 *Contributions to Mineralogy and Petrology* 143, no. 3 (2002): 300-315.
825
826 Girona, T., and F. Costa. "Dipra: A User-Friendly Program to Model Multi-Element
827 Diffusion in Olivine with Applications to Timescales of Magmatic Processes."
828 *Geochemistry Geophysics Geosystems* 14, no. 2 (2013): 422-431.
829
830 Grove, T. L., L. T. Elkins-Tanton, S. W. Parman, N. Chatterjee, O. Muntener, and G. A.
831 Gaetani. "Fractional Crystallization and Mantle-Melting Controls on Calc-Alkaline
832 Differentiation Trends." *Contributions to Mineralogy and Petrology* 145, no. 5
833 (2003): 515-533.
834
835 Gualda, G. A. R., M. S. Ghiorso, R. V. Lemons, and T. L. Carley. "Rhyolite-Melts: A
836 Modified Calibration of Melts Optimized for Silica-Rich, Fluid-Bearing Magmatic
837 Systems." *Journal of Petrology* 53, no. 5 (2012): 875-890.
838
839 Haase, K. A., N. Stroncik, D. Garbe-Schnoberg, and P. Stoffers. "Formation of Island Are
840 Dacite Magmas by Extreme Crystal Fractionation: An Example from Brothers

841 Seamount, Kermadec Island Arc (Sw Pacific)." *Journal of Volcanology and*
842 *Geothermal Research* 152, no. 3-4 (2006): 316-330.
843
844 Haase, K. M., S. Krumm, M. Regelous, and M. Joachimski. "Oxygen Isotope Evidence for
845 the Formation of Silicic Kermadec Island Arc and Havre-Lau Backarc Magmas by
846 Fractional Crystallisation." *Earth and Planetary Science Letters* 309, no. 3-4 (2011):
847 348-355.
848
849 Harford, C.L., Pringle, M.S., Sparks, R.S.J., Young S.R. "The Volcanic Evolution of
850 Montserrat Using ^{40}ar/^{39}ar Geochronology." In *The Eruption of Soufrière Hills*
851 *Volcano, Montserrat, from 1995 to 1999*, edited by T.H. Druitt, Kokelaar, B.P., 21,
852 93-113. London: Geological Society of London Memoirs, 2002.
853
854 Hauri, E., J. H. Wang, J. E. Dixon, P. L. King, C. Mandeville, and S. Newman. "Sims
855 Analysis of Volatiles in Silicate Glasses 1. Calibration, Matrix Effects and
856 Comparisons with Ftir." *Chemical Geology* 183, no. 1-4 (2002): 99-114.
857
858 Hautmann, S., A. G. Camacho, J. Gottsmann, H. M. Odbert, and R. T. Syers. "The Shallow
859 Structure beneath Montserrat (West Indies) from New Bouguer Gravity Data."
860 *Geophysical Research Letters* 40, no. 19 (2013): 5113-5118.
861
862 Hildreth, W. (1981). Gradients in silicic magma chambers – Implications for lithospheric
863 magmatism. *Journal of Geophysical Research* **86**, 153-192.
864

Horwell, C. J., L. P. Brana, R. S. J. Sparks, M. D. Murphy, and V. L. Hards. "A Geochemical Investigation of Fragmentation and Physical Fractionation in Pyroclastic Flows from the Soufriere Hills Volcano, Montserrat." *Journal of Volcanology and Geothermal Research* 109, no. 4 (2001): 247-262.

Housh, T. B., and J. F. Luhr. "Plagioclase-Melt Equilibria in Hydrous Systems." *American Mineralogist* 76, no. 3-4 (1991): 477-492.

Humphreys, M. C. S., M. Edmonds, T. Christopher, and V. Hards. "Chlorine Variations in the Magma of Soufriere Hills Volcano, Montserrat: Insights from Cl in Hornblende and Melt Inclusions." *Geochimica Et Cosmochimica Acta* 73, no. 19 (2009): 5693-5708.

Humphreys, M. C. S., M. Edmonds, T. Christopher, and V. Hards. "Magma Hybridisation and Diffusive Exchange Recorded in Heterogeneous Glasses from Soufriere Hills Volcano, Montserrat." *Geophysical Research Letters* 37, (2010).

Humphreys, M. C. S., M. Edmonds, M. Plail, J. Barclay, D. Parkes, and T. Christopher. "A New Method to Quantify the Real Supply of Mafic Components to a Hybrid Andesite." *Contributions to Mineralogy and Petrology* 165, no. 1 (2013): 191-215.

Hutton, D. H.W., and Reavey, M. A.,. "Strike-Slip Tectonics and Granite Petrogenesis:." *Tectonics* 11, (1992): 960-967.

Jurewicz, A. J. G., and E. B. Watson. "Cations in Olivine .1. Calcium Partitioning and Calcium-Magnesium Distribution between Olivines and Coexisting Melts, with Petrologic Applications." *Contributions to Mineralogy and Petrology* 99, no. 2 (1988): 176-185.

Karlstrom, L., Dufek, J. & Manga, M. (2009). Organization of volcanic plumbing through magmatic lensing by magma chambers and volcanic loads. *Journal of Geophysical Research: Solid Earth* **114**, B10204.

Katsui, Y., Ōba, Y., Ando, S., Nishimura, S., Masuda, H., Kurasawa, H. & Fujimaki, H. (1978). Petrochemistry of the Quaternary volcanic rocks of Hokkaido, north Japan. *Journal of the Faculty of Science, Hokkaido University. Series 4, Geology and mineralogy* **18**, 449 - 484.

Katsui, Y., Yamamoto, M., Nemoto, S. & Niida, K. (1979). Genesis of calc-alkalic andesite from oshima-oshima and ichinomegata volcanoes, north Japan. *Journal of the Faculty of Science, Hokkaido University. Series 4, Geology and mineralogy* **19**, 157 - 168.

Kent, A. J. R. (2008). Melt Inclusions in Basaltic and Related Volcanic Rocks. In: Putirka, K. D. & Tepley, F. J. (eds.) *Minerals, Inclusions and Volcanic Processes*, 273-331.

Kent, A. J. R., C. Darr, A. M. Koleszar, M. J. Salisbury, and K. M. Cooper. "Preferential Eruption of Andesitic Magmas through Recharge Filtering." *Nature Geoscience* 3, no. 9 (2010): 631-636.

914 Kiddle, E. J., B. R. Edwards, S. C. Loughlin, M. Petterson, R. S. J. Sparks, and B. Voight.
915 "Crustal Structure beneath Montserrat, Lesser Antilles, Constrained by Xenoliths,
916 Seismic Velocity Structure and Petrology." *Geophysical Research Letters* 37, (2010):
917 6.
918
919 Kohut, E. & Nielsen, R. L. (2004). Melt inclusion formation mechanisms and compositional
920 effects in high-An feldspar and high-Fo olivine in anhydrous mafic silicate liquids.
921 *Contributions to Mineralogy and Petrology* **147**, 684-704.
922
923 Koleszar, A. M., Kent, A. J. R., Wallace, P. J. & Scott, W. E. (2012). Controls on long-term
924 low explosivity at andesitic arc volcanoes: Insights from Mount Hood, Oregon.
925 *Journal of Volcanology and Geothermal Research* **219**, 1-14.
926
927 Lange, R. A., H. M. Frey, and J. Hector. "A Thermodynamic Model for the Plagioclase-
928 Liquid Hygrometer/Thermometer." *American Mineralogist* 94, no. 4 (2009): 494-506.
929
930 Lecuyer, F., O. Bellier, A. Gourgaud, and P. M. Vincent. "Active Tectonics of North-East
931 Sulawesi (Indonesia) and Structural Control of the Tondano Caldera." *Comptes*
932 *Rendus De L Academie Des Sciences Serie Ii Fascicule a-Sciences De La Terre Et*
933 *Des Planetes* 325, no. 8 (1997): 607-613.
934
935 Libourel, G. "Systematics of Calcium Partitioning between Olivine and Silicate Melt:
936 Implications for Melt Structure and Calcium Content of Magmatic Olivines."
937 *Contributions to Mineralogy and Petrology* 136, no. 1-2 (1999): 63-80.
938

939 Longhi J, Walker D, Hays JF. "Fe and Mg in Plagioclase." *Proc 7th Lunar Sci Conf*, (1976):
940 1281-1300.
941
942 Lopez-Escobar, L., Frey, F. A. & Vergara, M. (1977). Andesites and high-alumina basalts
943 from the central-south Chile high Andes: Geochemical evidence bearing on their
944 petrogenesis. *Contributions to Mineralogy and Petrology* **63**, 199-228.
945
946 Macdonald, R., C. J. Hawkesworth, and E. Heath. "The Lesser Antilles Volcanic Chain: A
947 Study in Are Magmatism." *Earth-Science Reviews* 49, no. 1-4 (2000): 1-76.
948
949 Mann, C. P., P. J. Wallace, and J. Stix. "Phenocryst-Hosted Melt Inclusions Record Stalling
950 of Magma During Ascent in the Conduit and Upper Magma Reservoir Prior to
951 Vulcanian Explosions, Soufriere Hills Volcano, Montserrat, West Indies." *Bulletin of*
952 *Volcanology* 75, no. 2 (2013).
953
954 Marsh, B. D. (1980). Geology and petrology of northern Atka, Aleutian Islands, Alaska.
955 *Geological Society of America Bulletin - Abstracts with Programs* **12**, 476.
956
957 Martin, V. M., Morgan, D. J., Jerram, D. A., Caddick, M. J., Prior, D. J. & Davidson, J. P.
958 (2008). Bang! Month-scale eruption triggering at Santorini volcano. *Science* **321**,
959 1178-1178.
960
961 Mathieu, Lucie, Benjamin van Wyk de Vries, Martin Pilato, and Valentin R. Troll. "The
962 Interaction between Volcanoes and Strike-Slip, Transtensional and Transpressional

963 Fault Zones: Analogue Models and Natural Examples." *Journal of Structural Geology*
964 33, no. 5 (2011): 898-906.
965
966
967 Melekhova, E., C. Annen, and J. Blundy. "Compositional Gaps in Igneous Rock Suites
968 Controlled by Magma System Heat and Water Content." *Nature Geoscience* 6, no. 5
969 (2013): 385-390.
970
971 Milia, A., and M. M. Torrente. "Late-Quaternary Volcanism and Transtensional Tectonics in
972 the Bay of Naples, Campanian Continental Margin, Italy." *Mineralogy and Petrology*
973 79, no. 1-2 (2003): 49-65.
974
975 Millet, M. A., Tutt, C. M., Handler, M. R. & Baker, J. A. (2014). Processes and time scales of
976 dacite magma assembly and eruption at Tauhara volcano, Taupo Volcanic Zone, New
977 Zealand. *Geochemistry Geophysics Geosystems* **15**, 213-237.
978
979
980 Moore, M. J. "Tectonics of the Najd Transcurrent Fault System, Saudi Arabia." *Geological*
981 *Society[London] Journal* 136, (1979): 441-454.
982
983 Morgan, D. J., S. Blake, N. W. Rogers, B. DeVivo, G. Rolandi, R. Macdonald, and C. J.
984 Hawkesworth. "Time Scales of Crystal Residence and Magma Chamber Volume from
985 Modelling of Diffusion Profiles in Phenocrysts: Vesuvius 1944." *Earth and Planetary*
986 *Science Letters* 222, no. 3-4 (2004): 933-946.
987

Murphy, M. D., R. S. J. Sparks, J. Barclay, M. R. Carroll, and T. S. Brewer. "Remobilization of Andesite Magma by Intrusion of Mafic Magma at the Soufriere Hills Volcano, Montserrat, West Indies." *Journal of Petrology* 41, no. 1 (2000): 21-42.

Murphy, M. D., R. S. J. Sparks, J. Barclay, M. R. Carroll, A. M. Lejeune, T. S. Brewer, R. Macdonald, S. Black, and S. Young. "The Role of Magma Mixing in Triggering the Current Eruption at the Soufriere Hills Volcano, Montserrat, West Indies." *Geophysical Research Letters* 25, no. 18 (1998): 3433-3436.

Myers, J. D. & Marsh, B. D. (1981). Geology and petrogenesis of the Edgecumbe Volcanic Field, SE Alaska - The interaction of basalt and crust. *Contributions to Mineralogy and Petrology* **77**, 272-287.

Nakamura, M. (1995). Continous mixing of crystal mush and replenished magma in the ongoing Unzen eruption. *Geology* **23**, 807-810.

Nelson, S. T., and A. Montana. "Sieve-Textured Plagioclase in Volcanic-Rocks Produced by Rapid Decompression." *American Mineralogist* 77, no. 11-12 (1992): 1242-1249.

Newman, S., and J. B. Lowenstern. "Volatilecalc: A Silicate Melt-H2o-Co2 Solution Model Written in Visual Basic for Excel." *Computers & Geosciences* 28, no. 5 (2002): 597-604.

Pallister, J. S., R. P. Hoblitt, and A. G. Reyes. "A Basalt Trigger for the 1991 Eruptions of Pinatubo Volcano." *Nature* 356, no. 6368 (1992): 426-428.

Paulatto, M., T. A. Minshull, and T. J. Henstock. "Constraints on an Intrusive System beneath the Soufriere Hills Volcano, Montserrat, from Finite Difference Modeling of a Controlled Source Seismic Experiment." *Geophysical Research Letters* 37, (2010).

Pearce, J. A., P. E. Baker, P. K. Harvey, and I. W. Luff. "Geochemical Evidence for Subduction Fluxes, Mantle Melting and Fractional Crystallization beneath the South Sandwich-Island Arc." *Journal of Petrology* 36, no. 4 (1995): 1073-1109.

Pinel, V. & Jaupart, C. (2000). The effect of edifice load on magma ascent beneath a volcano. *Philosophical Transactions of the Royal Society of London Series a-Mathematical Physical and Engineering Sciences* **358**, 1515-1532.

Plail, M, Barclay, J, Humphreys, MCS, Edmonds, M, Herd, R & Christopher, T, ed. *Characterisation of Mafic Enclaves in the Erupted Products of Soufriere Hills Volcano, Montserrat 1995-2010*. Edited by G. Wadge, Robertson, R. & Voight, B, The Eruption of Soufriere Hills Montserrat from 2000 to 2010: The Geological Society of London, 2014.

Plank, T., and C. H. Langmuir. "An Evaluation of the Global Variations in the Major Element Chemistry of Arc Basalts." *Earth and Planetary Science Letters* 90, no. 4 (1988): 349-370.

Price, R. C., Gamble, J. A., Smith, I. E. M., Stewart, R. B., Eggins, S. & Wright, I. C. (2005). An integrated model for the temporal evolution of andesites and rhyolites and crustal

development in New Zealand's North Island. *Journal of Volcanology and Geothermal Research* **140**, 1-24.

Putirka, K. D. "Thermometers and Barometers for Volcanic Systems." In *Minerals, Inclusions and Volcanic Processes*, edited by K. D. Putirka and F. J. Tepley, 69, 61-120, 2008.

Rea, J.W. "The Volcanic Geology and Petrology of Montserrat, West Indies." *J. Geol. Soc. Lond.* 130, (1974): 341-366.

Rea, W.J., Baker, P.E.,. "The Geochemical Characteristics and Conditions of Petrogenesis of the Volcanic Rocks of the Northern Lesser Antilles — a Review." *Bull. Volcanol.* 43, (1980): 325–336.

Reubi, O., and J. Blundy. "A Dearth of Intermediate Melts at Subduction Zone Volcanoes and the Petrogenesis of Arc Andesites." *Nature* 461, no. 7268 (2009): 1269-U103.

Rudnick, R. L. "Making Continental-Crust." *Nature* 378, no. 6557 (1995): 571-578.

Ruprecht, P. & Cooper, K. M. (2012). Integrating the Uranium-Series and Elemental Diffusion Geochronometers in Mixed Magmas from Volcan Quizapu, Central Chile. *Journal of Petrology* **53**, 841-871.

Ruprecht, P., and G. Worner. "Variable Regimes in Magma Systems Documented in Palgioclase Zoning Patterns: El Misti Stratovolcano and Andahua Monogenetic

Cones." *Journal of Volcanology and Geothermal Research* 165, no. 3-5 (2007): 142-162.

Sisson, T. W., and T. L. Grove. "Experimental Investigations of the Role of H2o in Calc-Alkaline Differentiation and Subduction Zone Magmatism." *Contributions to Mineralogy and Petrology* 113, no. 2 (1993): 143-166.

Sisson, T. W., K. Ratajeski, W. B. Hankins, and A. F. Glazner. "Voluminous Granitic Magmas from Common Basaltic Sources." *Contributions to Mineralogy and Petrology* 148, no. 6 (2005): 635-661.

Spinks, K. D., V. Acocella, J. W. Cole, and K. N. Bassett. "Structural Control of Volcanism and Caldera Development in the Transtensional Taupo Volcanic Zone, New Zealand." *Journal of Volcanology and Geothermal Research* 144, no. 1-4 (2005): 7-22.

Streck, M.J. "Mineral Textures and Zoning as Evidence for Open System Processes." In *Minerals, Inclusions, and Volcanic Processes*, 69, 595 - 619, 2008.

Streck, M. J., M. A. Dungan, E. Malavassi, M. K. Reagan, and F. Bussy. "The Role of Basalt Replenishment in the Generation of Basaltic Andesites of the Ongoing Activity at Arenal Volcano, Costa Rica: Evidence from Clinopyroxene and Spinel." *Bulletin of Volcanology* 64, no. 5 (2002): 316-327.

Sugawara, T. "Ferric Iron Partitioning between Plagioclase and Silicate Liquid: Thermodynamics and Petrological Applications." *Contributions to Mineralogy and Petrology* 141, no. 6 (2001): 659-686.

Tibaldi, A. "The Role of Transcurrent Intraarc Tectonics in the Configuration of a Volcanic Arc." *Terra Nova* 4, no. 5 (1992): 567-577.

Wadge, G. "Comparison of Volcanic Production-Rates and Subduction Rates in the Lesser Anitlles and Central America." *Geology* 12, no. 9 (1984): 555-558.

Wadge, G., and J. B. Shepherd. "Segmentation of the Lesser Antilles Subduction Zone." *Earth and Planetary Science Letters* 71, no. 2 (1984): 297-304.

Westercamp, D., Mervoyer, B.,. "Les Series Volcaniques De La Martinique Et De La Guadeloupe (F.W.I.)." *Bull. Bur. Rech.Geol. Min., Sect.* 4, no. 4 (Fr) (1976): 229–242.

Woods, A.W., Cowan, A., 2009. Magma mixing triggered during volcanic eruptions. Earth Planet. Sci. Lett. 288, 132-137.

Zajacz, Z., Candela, P.A., Piccoli, P.M., Sanchez-Valle, C., 2012. The partitioning of sulfur and chlorine between andesite melts and magmatic volatiles and the exchange coefficients of major cations. Geochimica Et Cosmochimica Acta 89, 81-101.

Zellmer, G. F., C. J. Hawkesworth, R. S. J. Sparks, L. E. Thomas, C. L. Harford, T. S. Brewer, and S. C. Loughlin. "Geochemical Evolution of the Soufriere Hills Volcano, Montserrat, Lesser Antilles Volcanic Arc." *Journal of Petrology* 44, no. 8 (2003): 1349-1374.

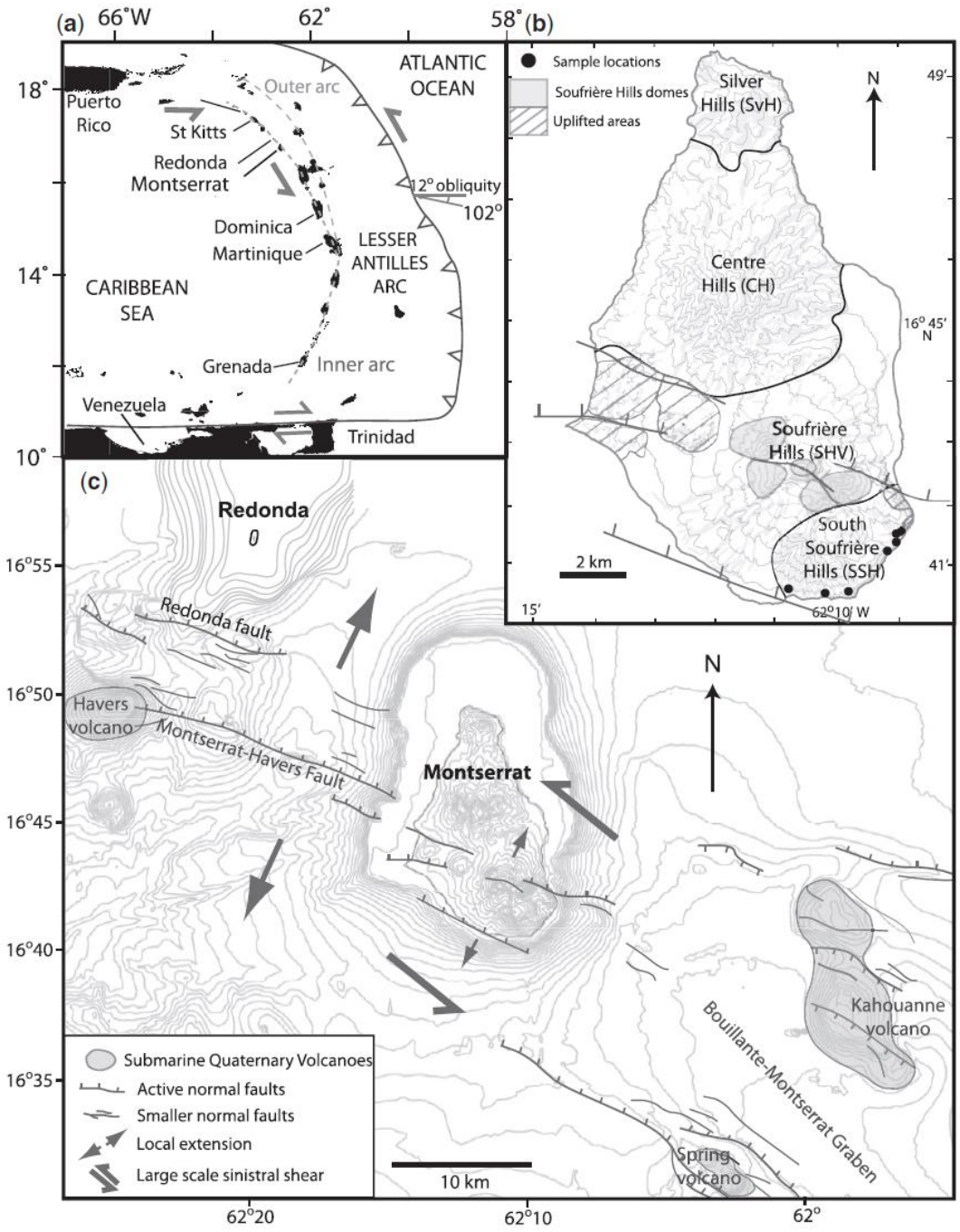

Fig. 1. (a) Regional map of the Lesser Antilles, showing oblique subduction and stresses. (b) The four volcanic centres of Montserrat, with locations of the sampled rocks from the SSH for this study indicated by the filled circles. (c) Submarine and subaerial faults and transtensional stresses in the region.

1118

Table 1: XRF bulk-rock data along with the standard Japanese Andesite 2 (JA-2), for localities and stratigraphic units sampled at the SSH

Latitude (N):	16·67672	16·67622	16·69131	16·69226	16·69005	16·69005	16·6769	JA-2	2 RSD
Longitude (W):	62·1693	62·1683	62·1487	62·1479	62·1488	62·1488	62·179		(%)
Stratigraphic unit:*	SSH B	SSH A	SSH A	SSH B	SSH A	SSH A	SSH A		
Sample name:	SSH3	SSH4	SSH5B	SSH10	SSH7G	SSH7B	SSH1F		
Major elements (wt %)									
SiO_2	49·22	50·87	58·77	48·06	47·84	50·19	52·69	56·35	0·2
TiO_2	1·00	0·87	0·59	0·97	0·90	0·77	0·87	0·65	1·7
Al_2O_3	18·67	19·20	17·95	18·89	19·30	19·67	17·63	15·64	2·1
Fe_2O_3	10·90	9·58	7·58	10·65	10·31	9·02	8·76	6·12	0·4
MnO	0·18	0·18	0·19	0·19	0·18	0·18	0·18	0·11	1·2
MgO	5·93	4·83	3·19	5·33	5·33	4·58	4·17	7·51	1·6
CaO	10·93	10·65	7·27	10·96	11·52	10·39	9·04	6·36	1·3
Na_2O	2·45	2·73	3·52	2·53	2·41	2·69	3·21	3·18	3·0
K_2O	0·63	0·69	0·60	0·59	0·53	0·34	0·77	1·85	3·3
P_2O_5	0·12	0·13	0·15	0·10	0·09	0·11	0·21	0·15	3·7
Total	100·0	99·7	99·8	98·3	98·4	97·9	97·5	99·2	

*According to Cassidy *et al.* (2012, 2014).

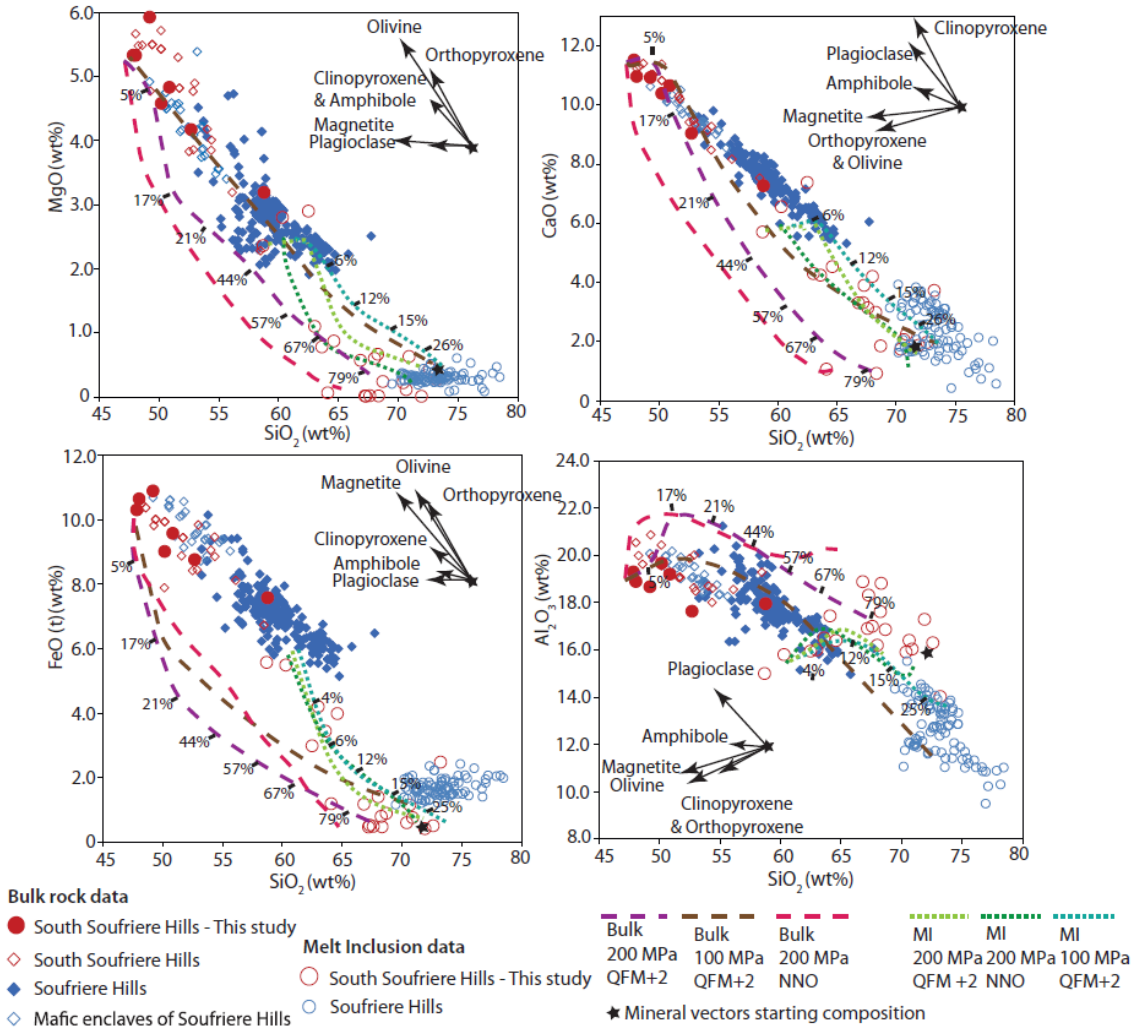

Fig. 2. Whole-rock variation diagrams from the Soufrière Hills, the mafic enclaves within the Soufrière Hills (SHV), the South Soufrière Hills (SSH), and the SSH samples used in this study. Data sources include Murphy *et al.* (1998, 2000), Horwell *et al.* (2001), Zellmer *et al.* (2003) and Cassidy *et al.* (2012). Dashed lines indicate fractional crystallization modelling under variable pressure and f_{O2} conditions.

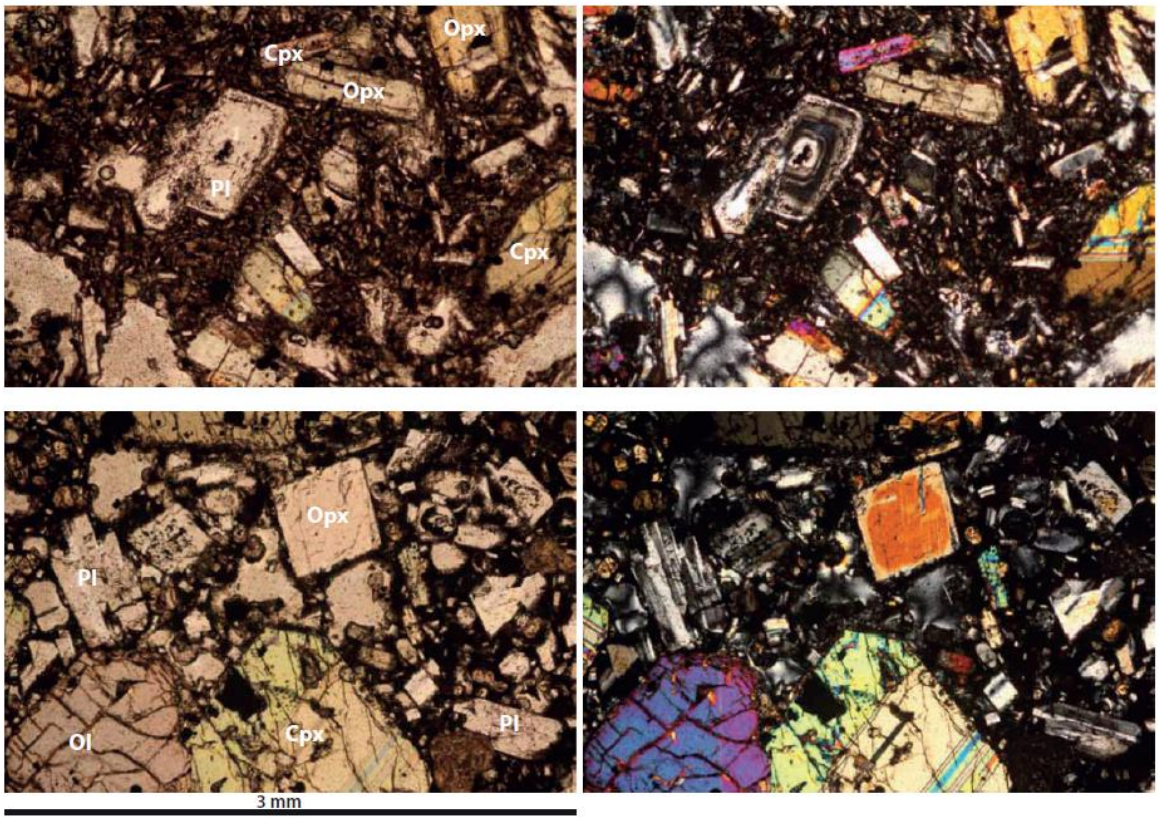

Fig. 3. Photomicrographs of two representative basalts, in plane-polarized light (left) and cross-polars (right). Each slide is 3 mm across. Some mineral phases are labelled: Cpx, clinopyroxene; Opx, orthopyroxene; Ol, olivine; Pl, plagioclase. Samples shown are 6_SSH1F (top) and 9_SSH4. The high crystallinity, large phenocrysts and features such as oscillatory zoning (e.g. plagioclase in top right photograph), normal zoning, twinning and sieve textures should be noted. Olivine is commonly large and fractured in appearance. Some pleochroism is present in clinopyroxenes.

1121

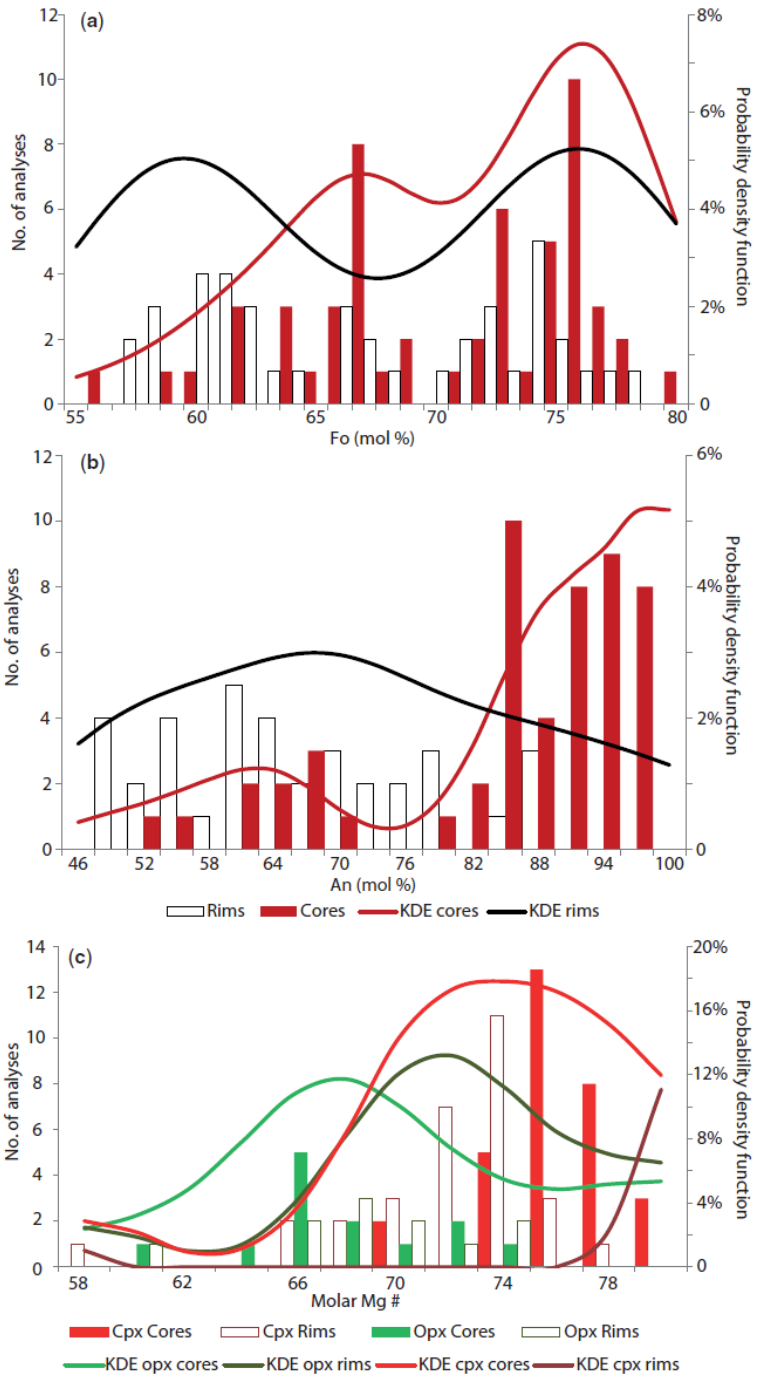

Fig. 4. Histograms to show the main crystal chemical ranges, including Kernel Density Estimation (KDE) curves, which correspond to the probability density function axis. (a) Distribution of forsterite content in olivines. (b) Anorthite distribution of cores and rims in plagioclase crystals. (c) Mg-number distribution of cores and rims in ortho- and clinopyroxene. The key for (a) and (b) is provided at the bottom of (b).

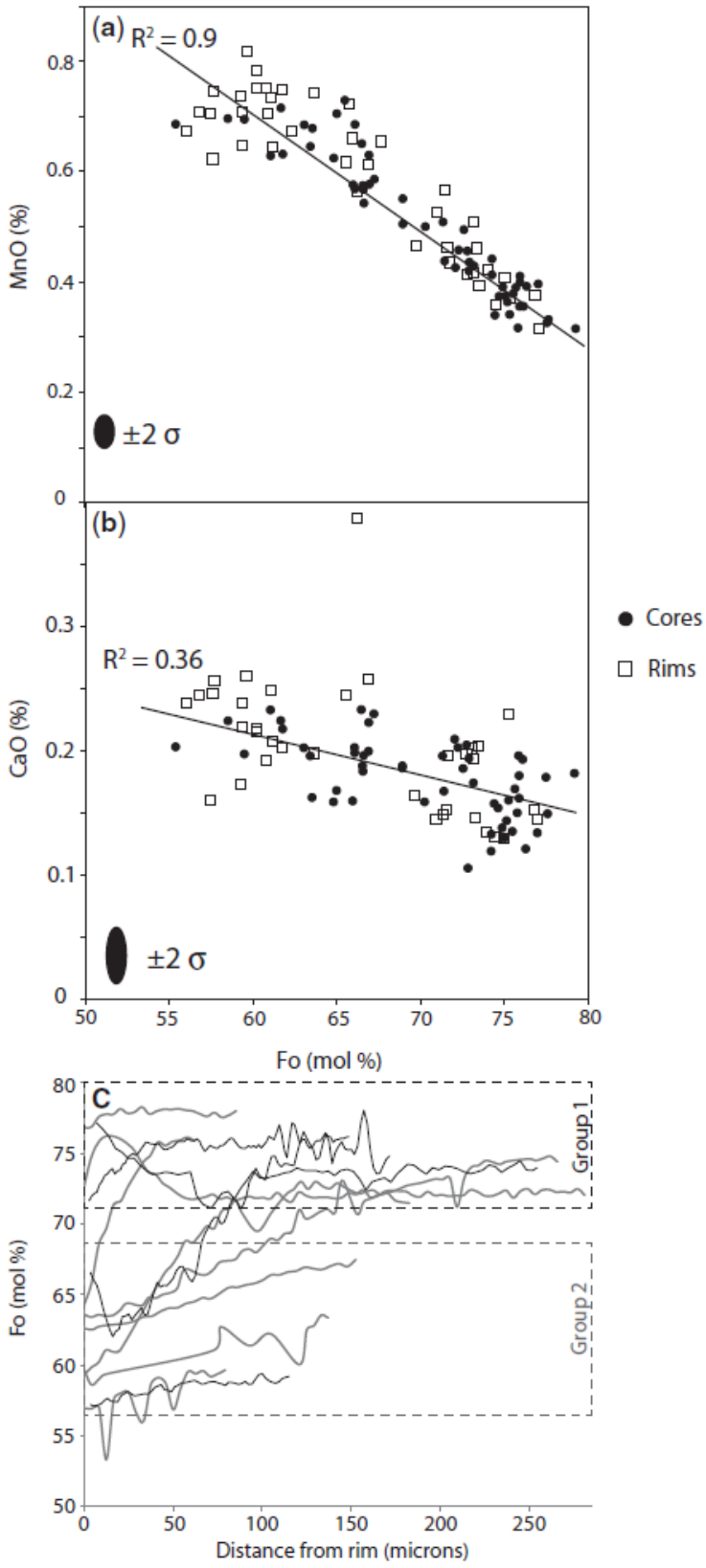

Fig. 5. (a, b) Point data plots of the chemical ranges in forsterite content against minor elements for olivines. (c) Zoning profiles for olivines. Black lines are traverses calculated by calibrated backscattered SEM images and grey lines are traverses measured directly with the electron microprobe.

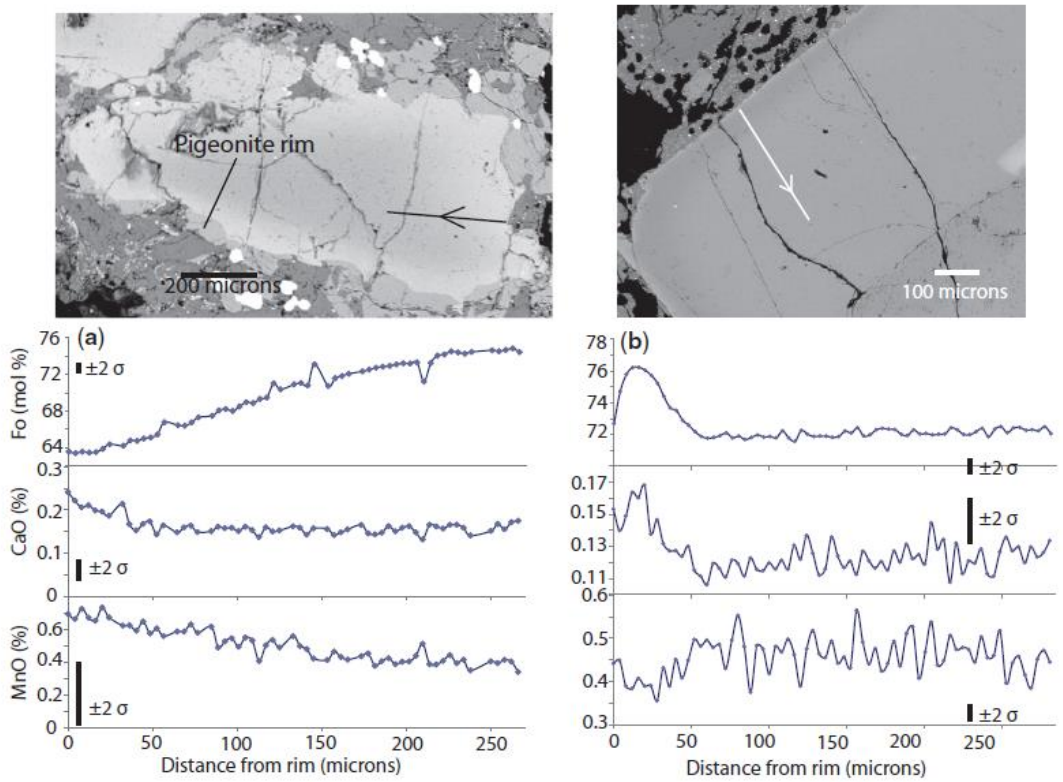

1124 **Fig. 6.** (a) Normally zoned olivine profile (9_SSH4_ol01); (b) complex zoned rim of an olivine (15_SSH7B_Ol02).

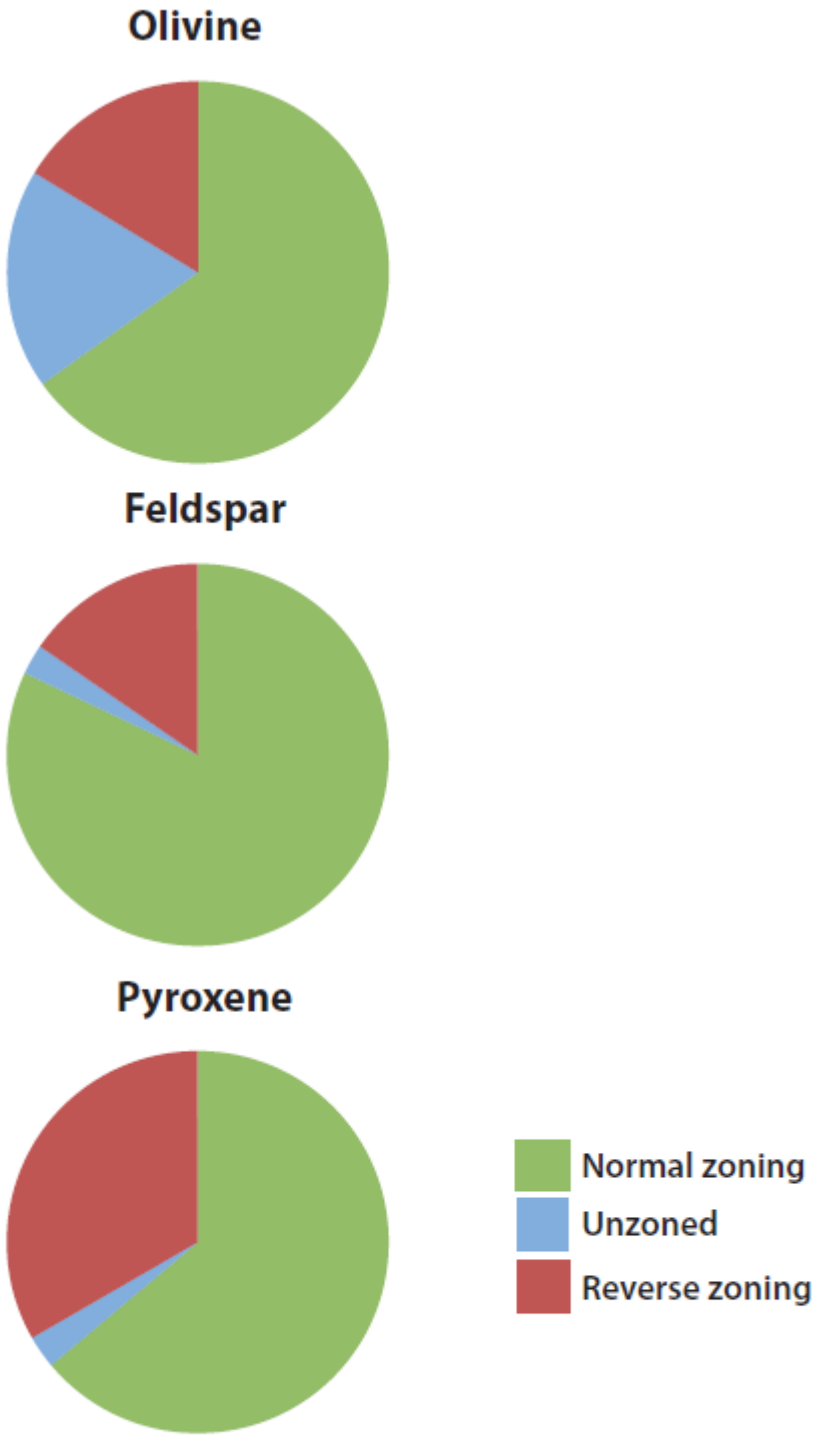

Fig. 7. Pie charts showing the proportion of crystals exhibiting normal, reverse or no zoning for olivine, plagioclase feldspars, and clino- and orthopyroxenes.

1125

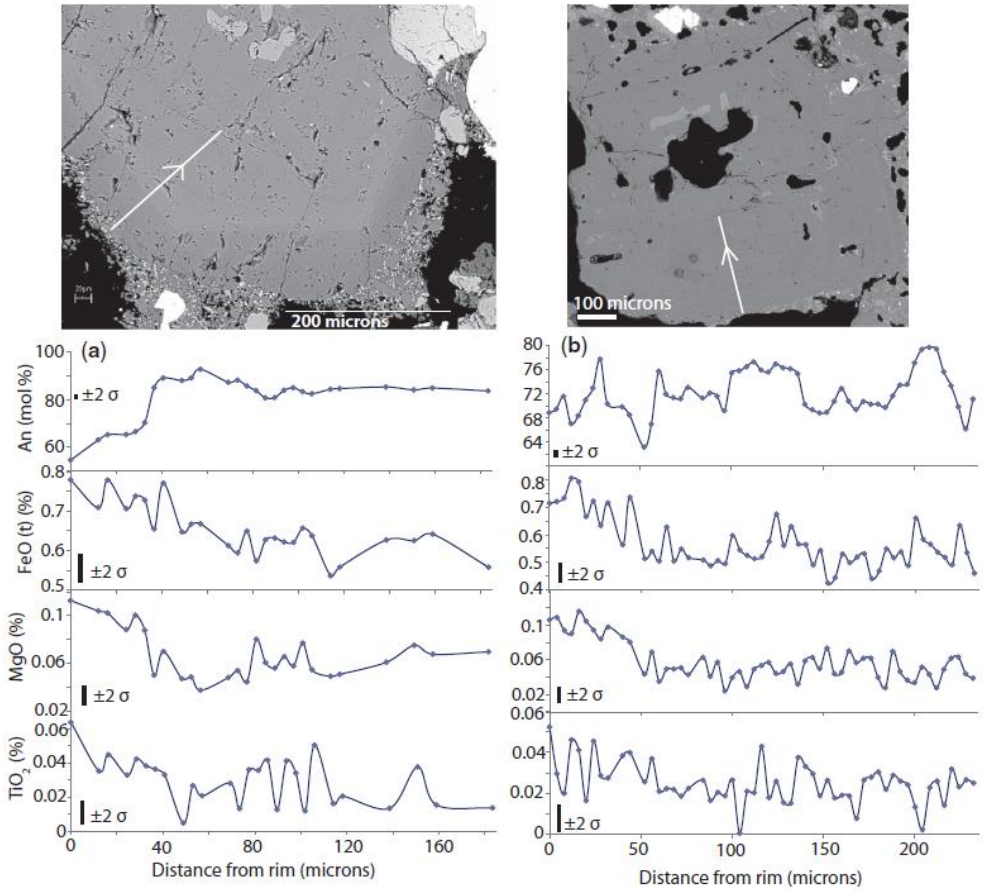

Fig. 8. Profiles of multi-element traverses showing plagioclase zoning: (a) s normal zoning of 9_SSH4Plag02; (b) demonstrates complex oscillatory zoning (15_SSH7BPlag02).

1126

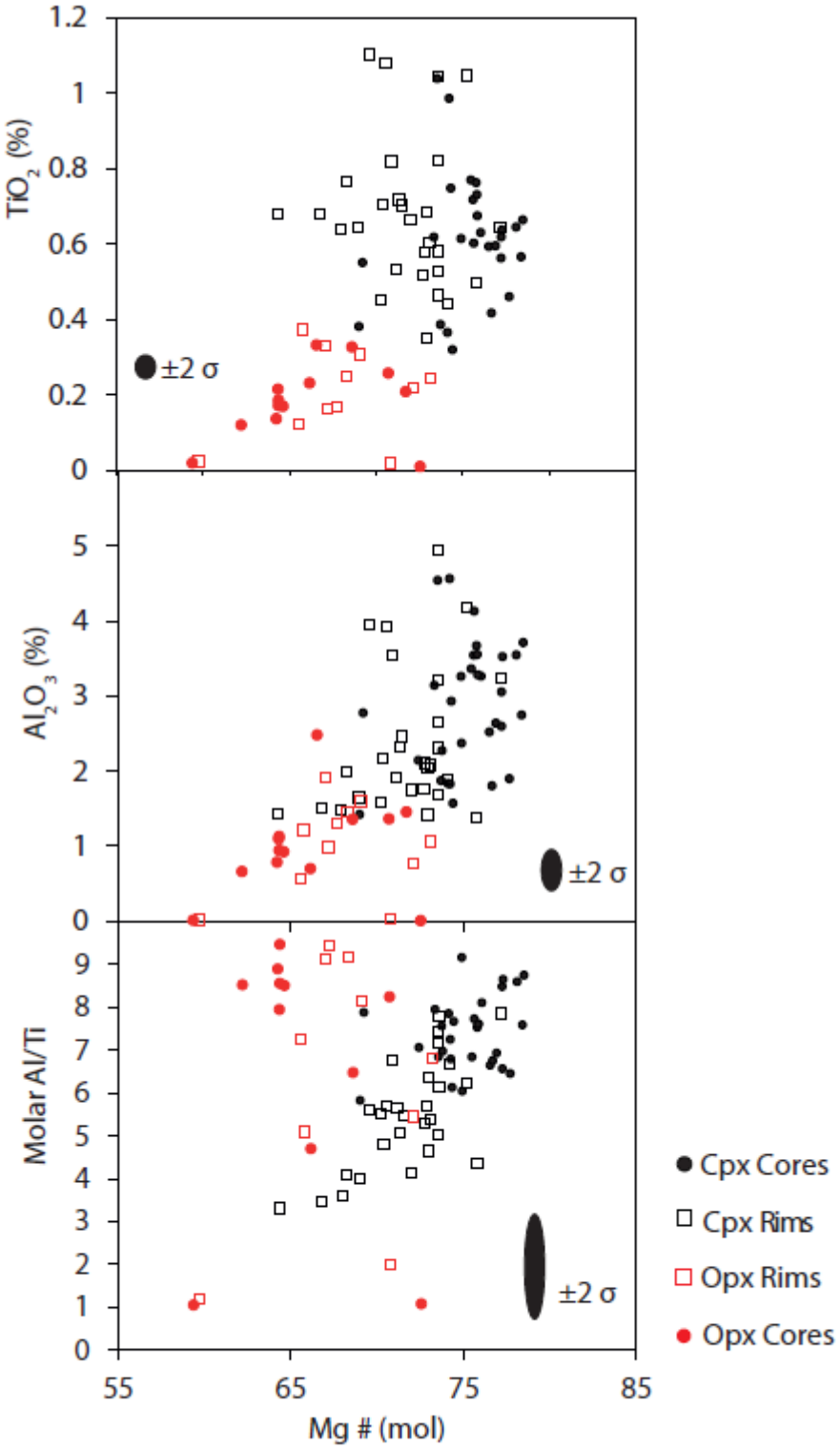

Fig. 9. Point data plots of the chemical ranges in Mg-number against minor elements for clino- and orthopyroxene.

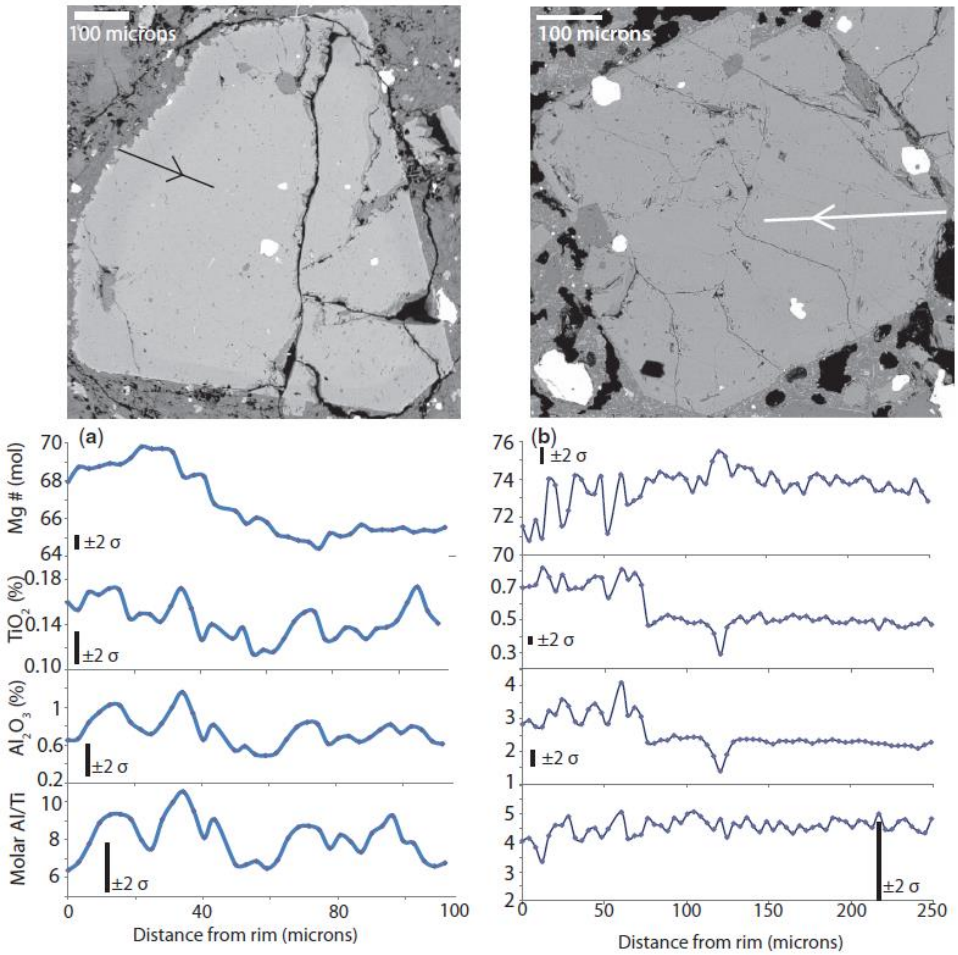

Fig. 10. Profiles of multi-element traverses showing pyroxene zoning: (a) reverse zoning of an orthopyroxene (12_SSH5Bopx09); (b) normal zoning of clinopyroxene (15_SSH7Bpyx02).

1128

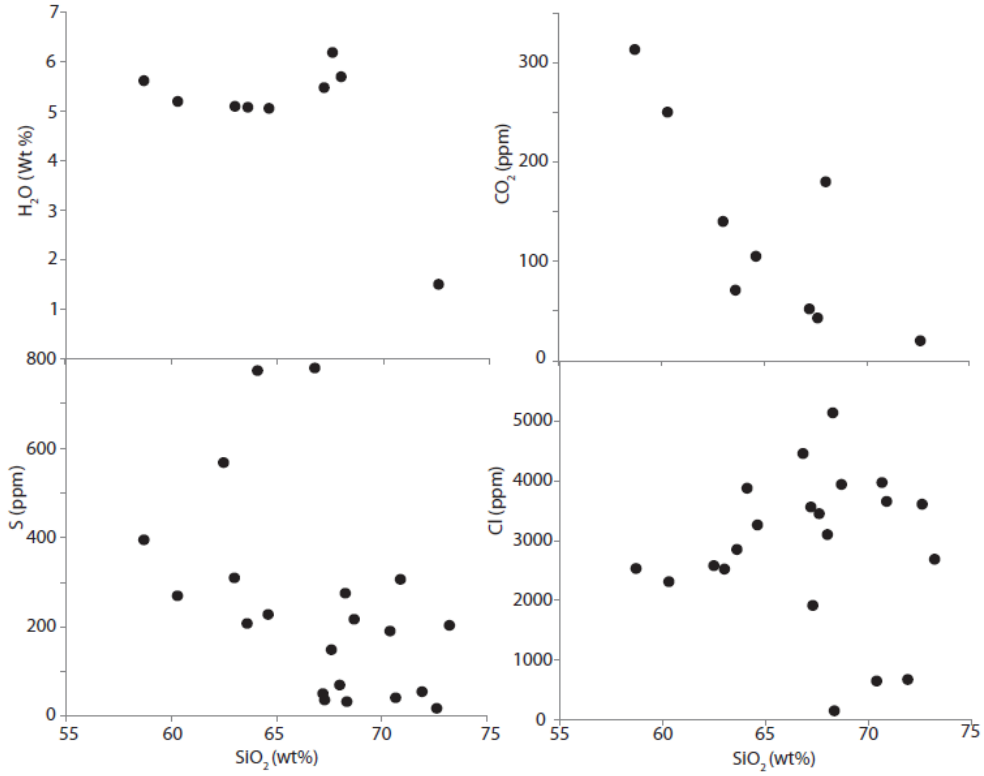

1129 **Fig. 11.** Melt inclusion plots, SiO_2 versus volatile contents.

Table 2: Major and volatile element compositions for melt inclusions analysed by electron microprobe and secondary ion mass spectrometry (SIMS) analysis

Sample	Phase	SiO_2	MgO	Al_2O_3	Na_2O	K_2O	CaO	TiO_2	Cr_2O_3	FeO_{tot}	Total	H_2O	CO_2	S	Cl	Mg# MI	Mg# host	K_D
SSH3	Pyx	72·60	0·44	16·30	4·91	2·61	1·97	0·22	b.d.	0·50	100·20	1·50	20	18	3610	67	79	0·54
SSH4	Pyx	64·60	0·87	16·40	4·08	1·05	4·53	0·86	0·009	3·98	97·00	5·06	105	228	3260	33	62	0·31
SSH4	Pyx	63·60	0·78	16·50	4·31	0·97	4·24	0·59	0·008	3·44	95·00	5·08	71	208	2850	34	63	0·31
SSH10	Ol	58·70	2·36	15·00	2·13	2·22	5·70	0·68	0·003	5·57	92·90	5·62	313	395	2530	49	77	0·29
SSH5B	Pyx	67·60	0·02	17·00	4·51	1·58	3·14	0·48	b.d.	0·48	95·40	6·19	43	149	3450	8·7	66	0·05
SSH5B	Pyx	67·20	0·01	16·90	4·49	1·60	3·31	0·70	b.d.	0·46	95·10	5·48	52	51	3560	4·8	65	0·03
SSH10	Ol	60·30	2·80	15·80	1·94	0·32	6·56	0·81	b.d.	5·49	94·00	5·20	250	270	2310	54	80	0·29
SSH5B	Pyx	68·00	0·60	16·20	4·20	1·60	4·20	0·41	0·006	1·40	96·60	5·70	180	70	3100	50	76	0·31
SSH4	Pyx	63·00	1·10	16·00	3·30	0·90	4·30	0·62	0·008	4·20	93·40	5·10	140	310	2520	38	65	0·32
SSH10	Pyx	68·33	0·01	18·82	6·12	7·55	0·92	0·04	b.d.	0·47	102·28			33	141	4·8	72	0·02
SSH4	Pyx	71·91	0·01	17·29	8·11	0·67	1·87	0·06	b.d.	0·41	100·42			55	667	3·6	73	0·01
SSH4	Pyx	68·68	0·24	16·86	3·92	4·78	1·85	0·57	0·004	0·89	98·47			217	3940	32	74	0·17
SSH4	Pyx	70·39	0·22	15·91	6·04	2·03	1·75	0·17	0·002	0·60	97·30			191	642	40	73	0·24
SSH4	Pyx	68·26	0·66	17·62	5·23	2·53	2·99	0·36	0·013	0·79	99·21			276	5142	60	73	0·56
SSH3	Pyx	64·10	0·06	17·43	3·70	7·92	1·07	0·59	b.d.	1·18	96·74			774	3877	8·5	71	0·04
SSH3	Pyx	70·88	0·63	16·04	5·31	2·15	2·24	0·38	0·006	0·76	98·99			307	3657	60	77	0·45
SSH3	Pyx	67·29	0·01	18·31	5·70	2·48	3·90	0·03	0·014	0·52	98·46			37	1910	3·0	75	0·01
SSH10	Pyx	70·65	0·11	16·41	4·35	3·09	2·06	0·88	0·002	1·15	102·93			42	3973	15	70	0·08
SSH3	Pyx	66·81	0·57	18·88	5·83	2·05	3·31	0·57	b.d.	1·17	100·02			780	4460	46	74	0·31
SSH3	Pyx	62·49	2·90	15·95	3·48	3·17	7·38	0·70	b.d.	2·98	99·55			568	2577	63	73	0·65
SSH5B	Pyx	73·21	0·28	14·03	3·65	2·26	3·73	0·57	b.d.	2·48	101·03			204	2685	17	67	0·10

All major element oxide concentrations are given in units of wt %; CO_2, S and Cl are given in ppm. FeO_{tot} denotes the FeO oxide concentration assuming that all Fe in the sample exists as Fe^{2+}. Mg# MI is the magnesium-number of the melt inclusion [molar Mg/(Mg + Fe)]; Mg# host is the magnesium-number of the crystal host (olivine, pyroxene—augite or enstatite); K_D is given by $(X_{Fe}/X_{Mg})_{host}/(X_{Fe}/X_{Mg})_{melt}$ (in moles), which is equal to $0{\cdot}3 \pm 0{\cdot}04$. Values outside this range indicate disequilibrium between melt inclusion and host (Roeder & Emslie, 1970). b.d., below detection limit.

1130

Table 3: Temperatures and pressures estimated using results of Putirka (2008)

Sample	T (°C)	An% or Mg# value	Method
11_SSH10_cpx04	1043	70·7	Two pyx
11_SSH10_opx06	1024	70·4	Two pyx
6_SSH1F_cpx04	970	69·0	Two pyx
14_SSH7G_plag01	1166	89·7	Plag–melt
14_SSH7G_plag06	1166	94·0	Plag–melt

Table 4: Equilibration pressures for melt inclusions trapped in clinopyroxene and olivine phenocrysts using the saturation models of Dixon et al. (1997) in VOLATILECALC (Newman & Lowenstern, 2004)

H_2O (wt %)	CO_2 (ppm)	T (°C)	H_2O_v (mol %)	CO_2 (mol %)	P (MPa)	Depth (km)
1·50	20	1000	86·8	13·2	26·8	1·2
5·06	105	1000	90·7	9·3	199·3	8·7
5·08	71	1000	93·5	6·5	193·9	8·4
5·62	313	1000	79·4	20·6	266·6	11·6
6·19	43	1000	97·0	3·0	247·1	10·7
5·48	52	1000	95·7	4·3	211·4	9·2
5·20	250	1000	81·1	18·9	233·7	10·2
5·70	180	1000	87·2	12·8	246·6	10·7
5·10	140	1000	88·1	11·9	208·0	9·0

Depths are estimated using a lithostatic pressure gradient of 23 MPa km^{-1} (Hautmann *et al.*, 2013).

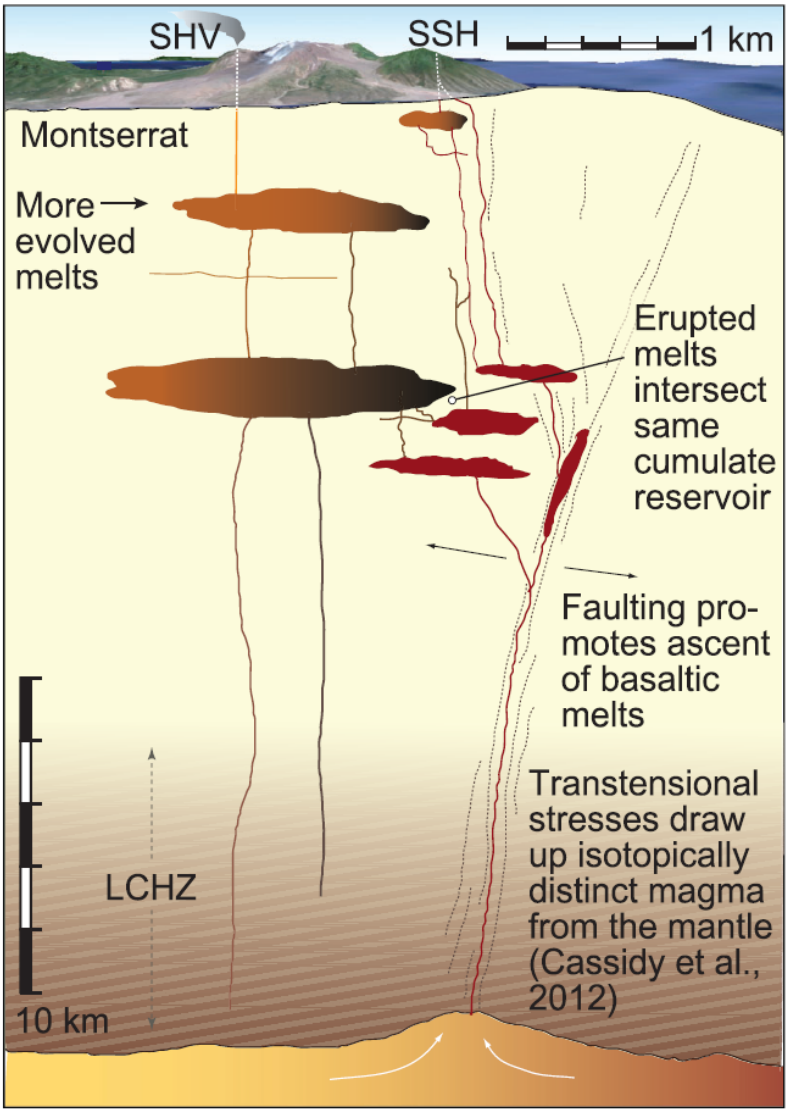

Fig. 12. Schematic figure showing how transtensional faulting can lead to the ascent of basaltic SSH magmas. The depths and processes involved in the generation of the SSH and SHV volcanism are shown. LCHZ, Lower Crustal Hot Zone of Annen *et al.* (2006).

1132